Negative microfilm 64–12,681
received from university

SHAKLEE, Francis Sowersby, 1935–
THE BRANCHING RATIOS OF THE POSITIVE K MESON.

The University of Michigan, Ph.D., 1964
Physics, nuclear

University Microfilms, Inc., Ann Arbor, Michigan

THE BRANCHING RATIOS OF THE POSITIVE K MESON

by
Francis Sowersby Shaklee

A dissertation submitted in partial fulfillment
of the requirements for the degree of
Doctor of Philosophy in The
University of Michigan
1964

Doctoral Committee:

Assistant Professor Byron P. Roe, Chairman
Professor Fred T. Haddock
Associate Professor Robert R. Lewis, Jr.
Assistant Professor Oliver E. Overseth, Jr.
Associate Professor Daniel Sinclair

TABLE OF CONTENTS

	Page
LIST OF TABLES	iii
LIST OF FIGURES	iv
I. INTRODUCTION	1
A. Previous Experiments	1
B. Theoretical Predictions	1
II. DATA COLLECTION	8
III. DATA REDUCTION	9
A. Scanning	9
B. Measuring	16
IV. DATA ANALYSIS	23
A. Monte Carlo Calculations	23
B. Biases	29
C. Bias Reduction	33
D. Bias Compensation	40
E. Calculating the Branching Ratios	50
V. RESULTS	56
A. Numbers Needed to Calculate the Branching Ratios	56
B. Summary of Results	56
C. Discussion	56
REFERENCES	65

LIST OF TABLES

Table		Page
I.	Previous Determinations of the K^+ Branching Ratios	2
II.	Probability of Passing $K_{\pi 2}$ Kinematics	21
III.	The Complete Set of Quantities Used to Calculate the Branching Ratios	57
IV.	Values of the Quantities Defined in Table III	58
V.	Comparison of the Present Experimental Results with Some Theoretical Predictions	59

LIST OF FIGURES

Figure		Page
1.	A τ decay.	11
2.	A K^+ decay identified as a two-gamma e^+.	12
3.	A K^+ decay identified as a four-gamma SD.	13
4.	The distribution of KINFIT for all the two-gamma events used in the present experiment.	20
5.	Curves showing how the distribution of KINFIT for the real $K_{\pi 2}$ events compares with the distribution of KINFIT for the simulated $K_{\pi 2}$ events.	30
6.	The distribution of Z-direction cosines for 66 gamma rays that were missed by the scanners and measurers.	36
7.	The distribution of Z-direction cosines for 650 gamma rays.	37
8.	The distribution of Z-direction cosines for all the ambiguous secondaries.	39
9.	Experimental and Monte Carlo energy distribution of the low energy gamma ray for $K_{\pi 2}$ decays.	41
10.	Kinematics of a K^+ stopping in xenon.	45
11.	Probability of a two-gamma $K_{\pi 2}$ passing $K_{\pi 2}$ kinematics as a function of the residual range cutoff.	47
12.	P(s), the probability that an electron secondary with potential path s will be recognized.	49
13.	Experimental solution of the theoretical equation for R.	64

I. INTRODUCTION

This section describes the relationship between the present experiment, previous experiments, and theoretical predictions.

A. Previous Experiments

The results of previous determinations of the K^+ branching ratios, along with the results of the present experiment, are summarized in Table I. The results of Birge et al.,[1] Alexander et al.,[2] and Taylor et al.[3] are from emulsion measurements. In the present experiment, a 12-in. xenon bubble chamber was exposed to a separated 700 MeV/c K^+ beam at the Bevatron (see Section II for further details). The results of Roe et al.,[4] were based on a preliminary analysis of approximately 25% of the usable film obtained in this exposure. The purpose of the present experiment is to analyze and report on the remaining film.

B. Theoretical Predictions

The numbers which are of particular interest to present theories are the ratios of the rates of $K_{\mu 3}$ to K_{e3}, τ' to τ, and $K_{\mu 2}$ to all K^+ decays.

TABLE I

PREVIOUS DETERMINATIONS OF THE K^+ BRANCHING RATIOS
(PERCENT)

Decay Mode	Birge et al.[a]	Alexander et al.[b]	Taylor et al.[c]	Roe et al.[d]	Present Experiment
$K_{\mu 2} \rightarrow \mu^+ + \nu$	58.5 ± 3.0	56.9 ± 2.6		64.2 ± 1.3	63.0 ± 0.8
$K_{\pi 2} \rightarrow \pi^+ + \pi^\circ$	27.7 ± 2.7	23.2 ± 2.2		18.6 ± 0.9	22.4 ± 0.8
$K_{\mu 3} \rightarrow \mu^+ + \pi^\circ + \nu$	2.8 ± 1.0	5.9 ± 1.3	2.8 ± 0.4	4.8 ± 0.6	3.0 ± 0.5
$K_{e3} \rightarrow e^+ + \pi^\circ + \nu$	3.2 ± 1.3	5.1 ± 1.3		5.0 ± 0.5	4.7 ± 0.3
$\tau^+ \rightarrow 2\pi^+ + \pi^-$	5.6 ± 0.4	6.8 ± 0.4	5.2 ± 0.3	5.7 ± 0.3	5.1 ± 0.2
$\tau^{+\prime} \rightarrow \pi^+ + 2\pi^\circ$	2.1 ± 0.5	2.2 ± 0.4	1.5 ± 0.2	1.7 ± 0.2	1.8 ± 0.2
$K_{\mu 3}/K_{e3}$	0.88 ± 0.47	1.16 ± 0.39		0.96 ± 0.15	0.63 ± 0.10
$\tau^{+\prime}/\tau^+$	0.375 ± 0.093	0.324 ± 0.062	0.288 ± 0.042	0.298 ± 0.038	0.350 ± 0.039

[a]See Ref. 1.
[b]See Ref. 2.
[c]See Ref. 3.
[d]See Ref. 4

1. $K_{\mu 3}/K_{e3}$ RATIO

The three-body leptonic decay modes of the K^+ meson, $K^+ \rightarrow \mu^+ + \pi^\circ + \nu(K_{\mu 3})$ and $K^+ \rightarrow e^+ + \pi^\circ + \nu(K_{e3})$, are presently assumed to be governed by a decay interaction that is the product of a leptonic current, restricted just to vector (V) and axial vector (A) couplings, and a strangeness nonconserving current due to strongly interacting particles. In the approximation that the lepton and neutrino arise from a local interaction, the matrix element for the leptonic decay of the K^+ meson is[5]

$$\left[\frac{1}{2}(P_k+P_\pi)f_+ + \frac{1}{2}(P_k-P_\pi)f_-\right] \overline{U}(P_\nu)\gamma_\lambda(1+\gamma_5)V(P_L)$$

where P_π and P_k are the pion and kaon four-momenta, U and V are the Dirac spinors for the leptons, and f_+ and f_- can be scalar functions (called form factors) of $q^2 = (P_k-P_\pi)^2$, the square of the invariant four-momentum transfer. Since $\vec{P}_k = 0$ in the laboratory, f_+ and f_- can be considered functions only of the pion momentum. If the weak interaction is time-reversal invariant, f_-/f_+ must be real. The ratio f_-/f_+ determines the ratio of the total transition probabilities for $K^+_{\mu 3}$ and K^+_{e3} in accordance with[6]

$$R = \frac{W(K^+_{\mu 3})}{W(K^+_{e3})} = 0.651 + 0.126(f_-/f_+) + 0.0189(f_-/f_+)^2$$

assuming that f_+ and f_- vary slowly with q^2. It has also been shown[7] that on the basis of an S-wave K-π resonance at 880 MeV, R = 0.69, and

for a P-wave resonance at 880 MeV, R = 0.64.

The value of R obtained in the previous experiments is considered to be too high by some theorists.[7,8] It will be seen that the present experiment gives a lower value of R which is consistent with $f_- = 0$. This will be discussed further in Section V (Results).

2. τ'/τ RATIO

The three-pion decays of the K^+ meson afford an opportunity to check the $\Delta T = 1/2$ rule. The K^+ meson is in the isospin state $|T,T_z> = |1/2, 1/2>$. Assuming the $\Delta T = 1/2$ rule, the three pions must be in the isospin state $|1,1>$. From the fact that the K spin is zero, the generalized Pauli principle says that the three-pion isospin state must be symmetric. The only symmetric $|1,1>$ state for three pions is[9]

$$|1,1> = \sqrt{\frac{1}{15}}\{2[(-++) + (+-+) + (++-)] - [(00+) + (0+0) + (+00)]\}$$

where (-++) means $\pi^-(1)\pi^+(2)\pi^+(3)$, etc. Thus the amplitudes for τ' and τ decays are 1 and 2, respectively, and hence the ratio of the decay rates is 1/4. The correction for the difference in phase space in the τ' and τ decay modes contributes a factor[10] of 1.298, making the ratio of the τ' and τ decay rates equal to

$$\frac{W(\tau')}{W(\tau)} = \frac{1}{4}(1.298) = 0.325$$

3. $K_{\mu 2}$ BRANCHING RATIO

Consider the decays

$$\pi^{\pm} \to e^{\pm} + \nu \qquad K^{\pm} \to e^{\pm} + \nu \ (K_{e2})$$

$$\to \mu^{\pm} + \nu \qquad \to \mu^{\pm} + \nu \ (K_{\mu 2})$$

Assuming a two-component left-handed neutrino, the usual way of writing the decay matrix elements is

$$\frac{1}{\sqrt{2E}} C[\bar{U}_e \text{ or } \mu P_\lambda \gamma_\lambda (1+\gamma_5) V_\nu]$$

where E and P_λ are the energy and momentum respectively of the $\pi^{\pm}$ or $K^{\pm}$, $U_{e \text{ or } \mu}$ and V_ν are the free Dirac spinors for the leptons, and C is an arbitrary constant which may or may not be taken to be complex. The inner product, $P_\lambda \gamma_\lambda$, can be taken outside, giving

$$\frac{1}{\sqrt{2E}} Cm[\bar{U}_e \text{ or } \mu (1+\gamma_5) V_\nu]$$

where m is the mass of $e^{\pm}$ or $\mu^{\pm}$. This matrix element can be used to calculate the branching ratios of $\pi \to e + \nu$ to $\pi \to \mu + \nu$ and $K \to e + \nu$ to $K \to \mu + \nu$. The results are[11]

$$\frac{W(\pi \to e+\nu)}{W(\pi \to \mu+\nu)} = \left(\frac{m_e}{m_\mu}\right)^2 \left[\frac{1-(m_e/M_\pi)^2}{1-(m_\mu/M_\pi)^2}\right]^2 = 1.29 \times 10^{-4}$$

and

$$\frac{W(K\to e+\nu)}{W(K\to\mu+\nu)} = \left(\frac{m_e}{m_\mu}\right)^2 \left[\frac{1-(m_e/M_k)^2}{1-(m_\mu/M_k)^2}\right]^2 = 0.257 \times 10^{-4}$$

which are consistent with experiments.

Sugawara[12] suggests that in the above decay-matrix elements, the constant C be written

$$C = \frac{a}{M}$$

where M is the mass of $\pi^\pm$ or $K^\pm$, and a is a dimensionless constant. If the constant a is called a_π for the above π decays, and a_k for the above K decays, the above branching ratios are not affected because a/M cancels out. However, if one calculates the branching ratio of $\pi \to \mu + \nu$ to $K \to \mu + \nu$, the a/M plays an important role. One gets

$$\frac{W(\pi\to\mu+\nu)}{W(K\to\mu+\nu)} = \left(\frac{a_\pi}{a_k}\right)^2 \frac{M_k}{M_\pi} \left[\frac{1-(m_\mu/M_\pi)^2}{1-(m_\mu/M_k)^2}\right]^2 = 0.200\left(\frac{a_\pi}{a_k}\right)^2 \frac{M_k}{M_\pi}$$

The introduction of C = a/M causes an extra factor of $(M_k/M_\pi)^2$ which, when multiplied by the usual M_π/M_k term, gives the M_k/M_π factor shown in the above equation. Using 64% for the $K^\pm \to \mu^\pm + \nu$ to $K^\pm \to$ (all modes) branching ratio (the value obtained by Roe *et al.*[4]), $\tau_\pi = 2.55 \times 10^{-8}$ sec, and $\tau_k = 1.22 \times 10^{-8}$ sec, Sugawara discovered that

$$0.200\left(\frac{a_\pi}{a_k}\right)^2 \frac{M_k}{M_\pi} = \frac{1.22}{2.55}\,\frac{1}{.64}$$

or

$$\frac{a_\pi}{a_K} = 1.03$$

This means that the weak interaction appears to be universal in these leptonic decays in the sense that the constant a is the same for all these decay modes.

Taking into account the latest errors in lifetimes and masses,[13] one can calculate the $K_{\mu 2}$ branching ratio necessary to make $a_\pi/a_K = 1$. The result is 0.677 ± 0.011.

II. DATA COLLECTION

A 12-in. diam, 10-in. deep xenon bubble chamber was exposed to a separated beam of K^+ mesons of momentum 700 MeV/c at the Bevatron. A moderator was used to reduce the beam momentum to about 400 MeV/c when it entered the chamber, so that the K^+ mesons came to rest and decayed near the center of the chamber. The chamber had no magnetic field. Both the beam and the chamber have been described in detail elsewhere.[14-16] Xenon is a good liquid to use for studying K^+ decays because of its high efficiency for conversion of gamma rays from π° mesons into electron pairs and because of the ease of recognition of electrons in xenon.[17]

In the present experiment, about 10,600 4-view stereophotographs were used.

III. DATA REDUCTION

This section describes how the data were reduced from the original form, the stereophotographs, to the final form on magnetic tape. The data reduction was carried out with the help of the IBM 704, 709, and 7090 computers of The University of Michigan.

A. Scanning

1. INITIAL SCAN

The film was initially scanned twice by two independent professional scanners. For each K^+ decay, the following information was recorded:

a. Number of electron pairs from gamma rays associated with the decay (0 to 4).

b. Nature of the charged secondary. The charged secondaries were classified into the following categories:

(1) Two or three charged secondaries. The decay is a τ.

(2) e^+. The decay is a K_{e3}.

(3) N (nuclear). The secondary undergoes a nuclear interaction.

(4) SD (stop and decay). The secondary stops and decays in the chamber.

(5) N and SD. The secondary is both N and SD.

(6) OCT (out cannot tell). The secondary leaves the chamber and is neither SD, N, nor e^+.

The μ^+ secondary from a π^+ decay at rest has a range of only 1.3 mm in xenon and therefore cannot always be reliably identified. Thus no separation was made between stopping π and μ secondaries on the basis of π-μ decays.

Figure 1 shows a K^+ decay identified as a τ because it has three charged secondaries. The K^+ enters the chamber at A, stops at B, and decays into a $\pi^-(S_1)$ and two π^+'s (S_2 and S_3). The π^+'s can be seen to stop and subsequently decay in a π-μ-e sequence.

Figure 2 shows a K^+ decay classified as a two-gamma e^+. The K^+ enters the chamber at A, stops at B, and decays into an electron (E), recognized because of its large energy loss due to multiple scattering and also because of the bremsstrahlung at C. The two gamma rays convert at G_1 and G_2.

Figure 3 shows a K^+ decay classified as a four-gamma SD. The K^+ enters the chamber at A, stops at B, and decays into a secondary (S) that subsequently stops and decays in a π-μ-e sequence. The four gamma rays convert at G_1, G_2, G_3, and G_4.

When a scanner finished a roll of film, he punched his results on IBM cards according to a specific format. The punched cards of both scanners were placed together and run with a computer program called SCARE (scan and compare) which printed out the results of both

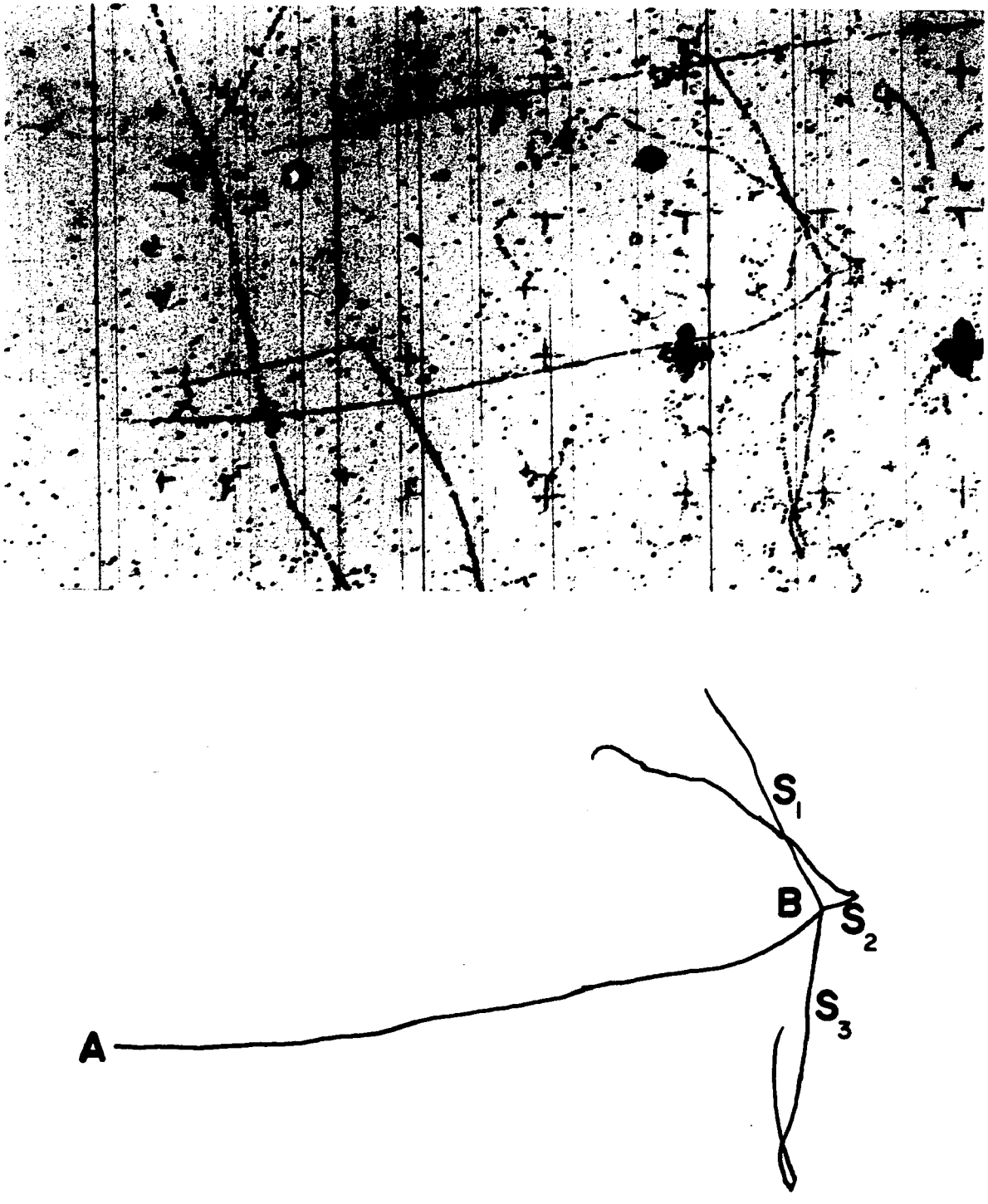


Figure 1. A τ decay. The K^+ enters the chamber at A, stops at B, and decays into a $\pi^-(S_1)$ and 2 π^+'s(S_2 and S_3). The π^+'s stop and decay in a π-μ-e sequence.

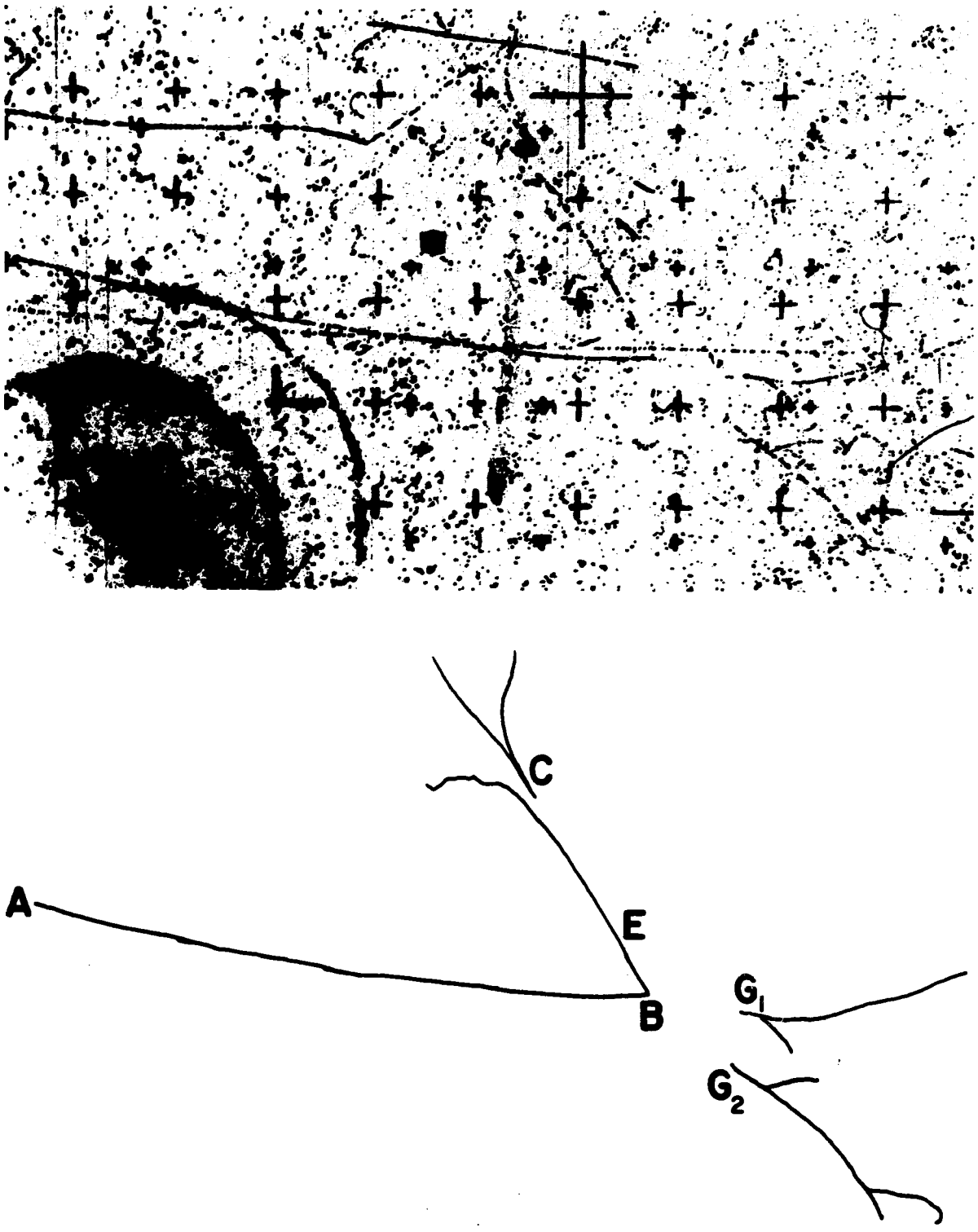


Figure 2. A K^+ decay identified as a two-gamma e^+. The K^+ enters the chamber at A, stops at B, and decays into an electron (E), recognized because of its large energy loss due to multiple scattering and also because of the bremsstrahlung at C. The two gamma rays convert at G_1 and G_2.

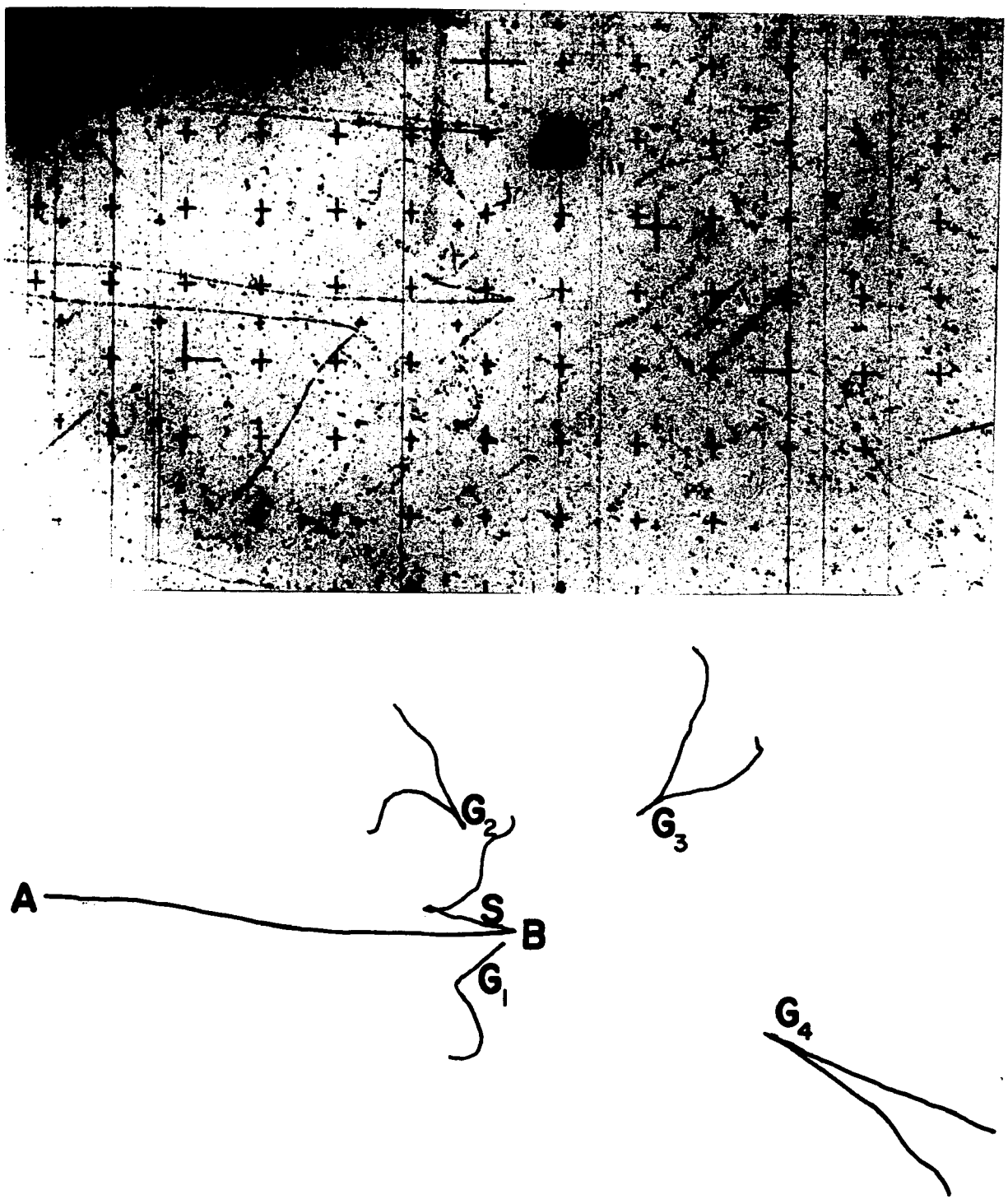


Figure 3. A K^+ decay identified as a four-gamma SD. The K^+ enters the chamber at A, stops at B, and decays into a secondary (S) that subsequently stops and decays in a π-μ-e sequence. The four gamma rays convert at G_1, G_2, G_3, and G_4.

scanners, making appropriate comments when disagreements were found. The events which were in disagreement were rescanned by the original scanners with the help of a physicist in order to resolve all disagreements. Each scanner corrected his own deck and the two decks were again run with the same computer program. This process was repeated until there were no disagreements between the scanners.

The reasons for checking the scanning results by machine instead of doing it by hand were twofold. First, the normal human errors involved in comparing two hand written lists and making a third corrected list were eliminated. Second, the computer output consisted of a neat list of all the events found in scanning, which could be placed in books and stored away for later consultation. The computer also printed out a table which gave the total number of events in each category, as well as a list of the events which were to be measured.

2. FINE SCAN

After the measuring phase of the experiment was completed (the measuring will be discussed later), the physicists decided that further scanning was necessary to evaluate and, if possible, reduce biases (biases will be discussed in Section IV). The plan was for two physicists to rescan, completely and independently, at least 10% of the film. Since this experiment is based on 53 reels of film, 5-1/2 reels were chosen to be rescanned. The choice was made in such a way that

the proportions of good, fair, and bad film were the same for the 5-1/2 reels as for the 53 reels. The results of the two physicists were compared and disagreements were ironed out.

On the remaining 47-1/2 reels of film, the physicists rescanned and checked the following events, provided the K^+ decay point was at least 5 cm from every wall of the chamber and the decay was not in flight.

a. All events for which the charged secondary was not an OCT.

b. All events which had two gamma rays convert in the chamber but failed the $K_{\pi 2}$ kinematical test (the $K_{\pi 2}$ kinematical test will be discussed later). The reason for checking these events was to see if the correct gamma rays had been measured.

Exceptions were τ decays, and decays classified as two-gamma nuclear, satisfying the $K_{\pi 2}$ kinematical test (such decays were assumed to be unquestionably $K_{\pi 2}$ decays). The rescanned events amounted to about 10% of all the events on the remaining 47-1/2 reels.

The physicists rescanned and checked approximately 20% of all the events used in the present experiment. How the fine scan results were used to evaluate and reduce biases will be discussed in Section IV.C and D. The events which the physicists found to be measured incorrectly were remeasured.

B. Measuring

1. EVENTS TO BE MEASURED

One of the outputs of the SCARE program was a list of events to be measured. All events found in scanning were to be measured, except τ decays, and decays classified as zero-gamma OCT. In addition, every tenth event found in scanning, regardless of its classification, was measured, in order to get an unbiased distribution of decay points in the chamber. This decay point distribution was used by the Monte Carlo programs as will be discussed in Section IV.A. The measured events amounted to about 36% of all the events found in scanning.

2. MEASURING MACHINES

Two measuring machines were used in the data reduction. The film stages in one machine were driven by precision screws accurate to 1μ/cm. The second machine used a Ferranti-Moiré fringe counter to determine the linear positions of the film stage to 0.0001 in. The output of each machine consisted of IBM cards punched with coded remarks describing the measured event, along with the projected stereo coordinates of the various points pertinent to the event.

It should be pointed out here that the accuracy of the measurements was limited not by the measuring machines but by the film, i.e., the bubble size, multiple scattering, decay configuration, etc. In fact, the measuring errors due to the film were, at best, roughly 12 times

the errors due to the measuring machines. The actual determination of these measuring errors will be discussed in Section IV.A.7.

3. THE MEASURING PROGRAM

The punched card output from the measuring machines was used by a computer program called KSORT3. The main job of KSORT3 was to convert the projected stereo coordinates into real space coordinates. The KSORT3 output was both printed on paper and punched on cards, and can be put into three classes: geometry, measurement quality, and kinematics.

a. Geometry. The geometrical quantities computed by KSORT3 were the space coordinates of the K^+ decay point, the conversion points of the gamma rays, and the points measured along the charged secondary to give its direction and range. These coordinates were all computed relative to an arbitrary origin in the chamber which was chosen to be the center grid-mark on the inside of the front window. Other geometrical quantities were the direction cosines, relative to the K^+ decay point, of the charged secondary and of the gamma rays that converted in the chamber.

b. Measurement quality. The measuring program, KSORT3, also computed some quantities that were an indication of the quality of the measurement. If a measurement did not meet specified

requirements with regard to measurement quality, appropriate comments were printed, and the event was put on a list of events to be remeasured.

c. Kinematics. K^+ decays which had exactly two gamma rays convert in the chamber were subjected to a kinematical test called the $K_{\pi 2}$ kinematical test, provided each of the two gamma rays converted at least 3 mm from the K^+ decay point. Decays which had one or more gamma rays convert less than 3 mm from the decay point were not subjected to the $K_{\pi 2}$ kinematical test because the gamma-ray direction cosines could not be determined accurately. It should be mentioned here that since the lifetime for $\pi^\circ \rightarrow 2\gamma$ is only about 10^{-16} sec, the π°'s never go more than 3×10^{-6} cm before decaying. Consequently, in the present experiment, the origin of all gamma rays can be taken as the K^+ decay point.

The decay configuration is completely specified by the direction cosines of each of the two gamma rays and the charged secondary, relative to the K^+ decay point. Since the $K_{\pi 2}$ decay mode is the only two-body decay mode having a π°, the idea of the $K_{\pi 2}$ kinematical test is to find out if the observed decay configuration could belong to a two-body decay. The first step was to check for coplanarity because in a $K_{\pi 2}$ decay with the K^+ at rest, the π^+ and the π° must go in opposite directions to conserve momentum. Consequently,

the initial π^+ direction must lie in the plane defined by the two gamma rays from the π°. Thus for the decay being tested, the angle between the direction of the charged secondary and the plane of the two gamma rays was computed. This angle was called DEVCOP (deviation from coplanarity) and was in degrees. The second step was to take the actual measured angle between the two gamma-ray directions and compute, using the constraints imposed by conservation of momentum and energy in a two-body decay, the direction in which the π^+ must go, provided the decay is really a $K_{\pi 2}$. The angle between this computed direction and the actual direction taken by the charged secondary was called ERFIT (fitting error) and was in degrees. The two angles, DEVCOP and ERFIT, were combined to form a single quantity called KINFIT (kinematics fit). KINFIT was arbitrarily defined to be the square root of the sum of the squares of DEVCOP and ERFIT.

Figure 4 is a histogram showing the variation of KINFIT for the two-gamma events used in the present experiment. An arbitrary cutoff of 8.5° for KINFIT was selected, meaning that all two-gamma events having KINFIT $\leq 8.5^\circ$ were said to pass $K_{\pi 2}$ kinematics, and all the two-gamma events having KINFIT $> 8.5^\circ$ were said to fail $K_{\pi 2}$ kinematics. Of all the two-gamma events used in the present experiment, excluding those iden-

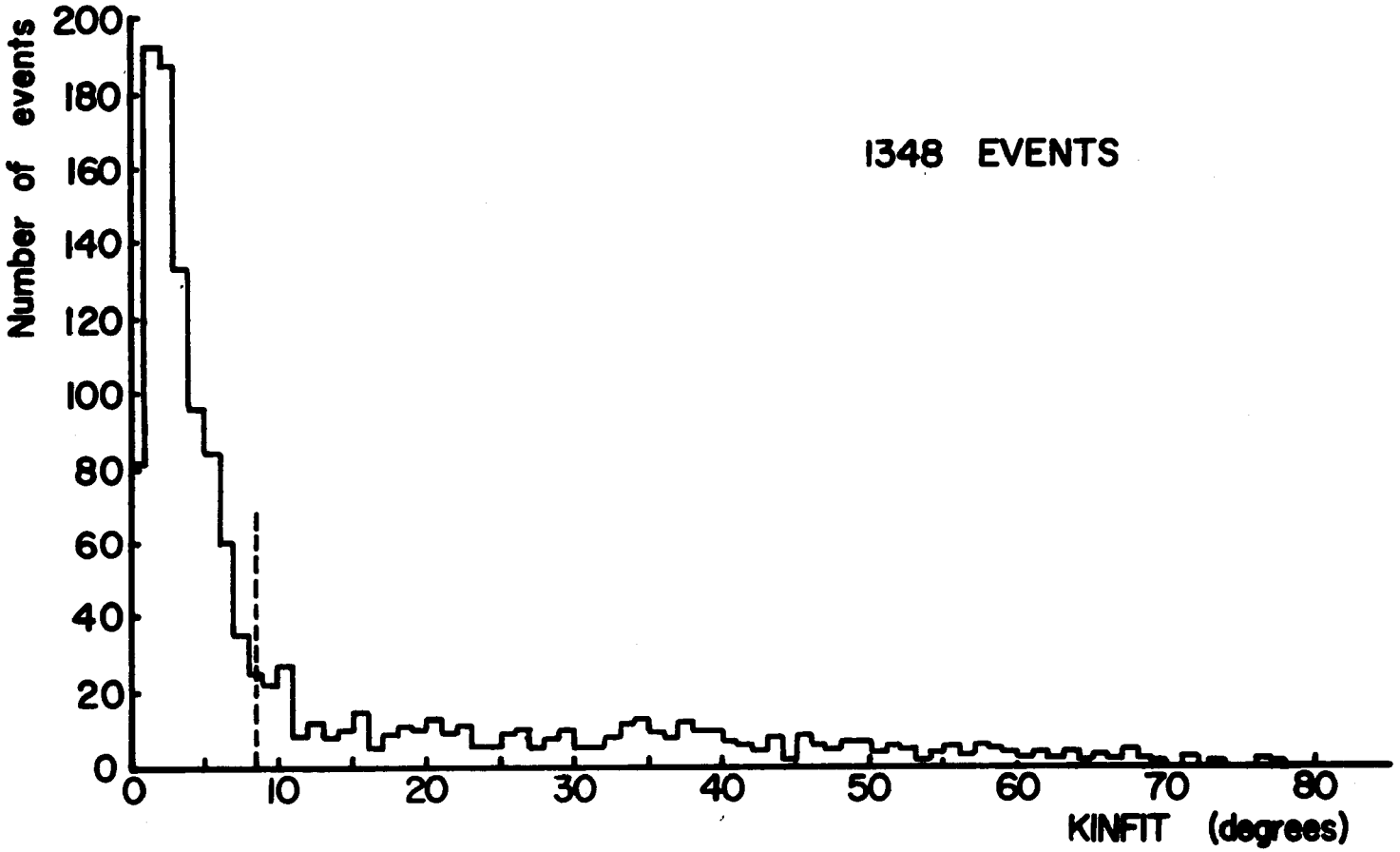


Figure 4. The distribution of KINFIT for all the two-gamma events used in the present experiment. The arbitrary borderline between events that pass and events that fail $K_{\pi 2}$ kinematics is represented by the dashed line at 8.5°.

tified in scanning as K_{e3} decays, 82.8% passed $K_{\pi 2}$ kinematics. Table II gives the probability that a two-gamma event of the indicated decay mode will pass $K_{\pi 2}$ kinematics.

TABLE II

PROBABILITY OF PASSING $K_{\pi 2}$ KINEMATICS

Decay Mode	Probability
$K_{\pi 2}$	0.925 ± 0.008
$K_{\mu 3}$	0.094 ± 0.002
K_{e3}	0.075 ± 0.002
τ'	0.013 ± 0.001

These probabilities were computed by a Monte Carlo procedure which will be discussed in Section IV.A. It should perhaps be mentioned here that the reason a two-gamma $K_{\pi 2}$ does not have a probability of 1.0 of passing $K_{\pi 2}$ kinematics is due to measurement errors, multiple scattering of the charged secondary, and decay in flight contamination. The reason for a small number of $K_{\mu 3}$, K_{e3}, and τ' decays passing $K_{\pi 2}$ kinematics is that the decay configurations just happened to be such that KINFIT was less than 8.5°.

4. DATA CHECK

After completion of the initial scanning, measuring, fine scan-

ning, and fine-scan remeasuring phases of the experiment, the data were thoroughly checked to see if any events had gotten lost. Such events were remeasured and added to the data. In addition, all events that were remeasured after the fine-scanning stage were checked to see if they were remeasured correctly. All corrected measurements were put into the KSORT3 output deck and the incorrect measurements were removed.

5. CARDS TO TAPE

The punched card output of the measuring program, KSORT3, contained essentially all of the information that was computed by KSORT3. The information about each K^+ decay occupied from one to fifteen punched cards. Each punched card contained the frame and decay number of the event to which it belonged. The total number of punched cards was approximately 36,000.

To facilitate further data handling, the KSORT3 output cards were read onto a magnetic tape according to a specified format. The final version of the magnetic tape was thoroughly tested to make sure that no errors had been made in the card to tape programs.

IV. DATA ANALYSIS

This section is designed to describe in detail how the data were used to calculate the K^+ branching ratios.

A. Monte Carlo Calculations

A large number of Monte Carlo $K_{\pi 2}$, $K_{\mu 3}$, K_{e3}, and τ' decays (all decays involving π°'s) were generated, using an IBM 7090 digital computer. The usefulness of this procedure will become clear to the reader later on as the results are used. The purpose of the following discussion is to show how the Monte Carlo events were made to simulate the real events as closely as possible.

1. RANDOM NUMBER GENERATION

Random numbers, uniformly distributed between 0 and 1, were obtained by means of the system subroutine called RANDOM(N), where N is the variable whose value is used to propagate the generation of random numbers. RANDOM employs the thoroughly tested power residue method of random number generation, with a periodicity of $2^{35} - 1$. The initial value of the argument, N, is obtained by performing a logical checksum of certain locations in low core, including the clock and various buffers, so that the probability of repeating the same sequence of random numbers on successive approaches to the machine is very small (less than 2×10^{-7}).

2. DECAY POINT DISTRIBUTION

An unbiased sample of 1000 decay points, obtained by measuring every tenth event found by the scanners, was used as the decay points of the Monte Carlo decays. One of these decay points was chosen at random for every Monte Carlo decay.

3. TRACK SEGMENT DISTRIBUTION

A representative sample of track segments (distance from the decay point to the first measured point on the charged secondary) was obtained from the following three kinds of events.

a. Events with electron secondaries.

b. Events with nonelectron secondaries and two electron pairs, passing the $K_{\pi 2}$ kinematical test.

c. Events with nonelectron secondaries and two electron pairs, failing the $K_{\pi 2}$ kinematical test.

The sample described in (a) is virtually 100% K_{e3} decays and was used to generate K_{e3} decays. The sample described in (b) is about 98% $K_{\pi 2}$ and was used to generate $K_{\pi 2}$ decays. The sample described in (c) contains the decay modes $K_{\mu 3}$, τ', $K_{\pi 2}$ is roughly the proportion 2:1:1 and was used to generate $K_{\mu 3}$ and τ' decays. A track segment from the appropriate sample was chosen at random for each Monte Carlo decay.

4. RADIATION LENGTH FORMULA

The following method was used to determine the conversion distance of gamma rays in xenon. The probability, $P(E,x)dx$, that a gamma ray of energy E will convert into an electron pair in xenon in a distance between x and x+dx is

$$P(E,x)dx = (1/L)\exp(-x/L)dx$$

L is called the radiation length for gamma rays and depends on the gamma ray energy according to the formula

$$L(E) = 5.1916 + \frac{136.906}{E} - \frac{1304.400}{E^2} + \frac{5558.646}{E^3}$$

which was developed by Dr. John L. Brown of the Lawrence Radiation Laboratory for use in the xenon bubble chamber. The formula is accurate to 1%.

5. COUPLING

In generating $K_{\mu 3}$ and K_{e3} decays, the π° momentum and the angle between the π° and the neutrino were obtained from the vector-axial vector coupling distribution, assuming variable form factors with the latest experimental energy dependence.[18] For τ' decays, phase space was assumed to govern the decay configuration.

6. THE TWO-GAMMA KINEMATICAL TEST

Those Monte Carlo decays that had exactly two gamma rays convert in the chamber were subjected to the same $K_{\pi 2}$ kinematical test that was described in Section III.B.3. The purpose was to ascertain the probabilities that two-gamma $K_{\pi 2}$, $K_{\mu 3}$, K_{e3}, and τ' decays will pass the $K_{\pi 2}$ kinematical test. The results are given in Table II, P.21.

7. MEASUREMENT ERROR PERTURBATION

To subject a Monte Carlo event with two gamma rays converting in the chamber to the $K_{\pi 2}$ kinematical test (see Section III.B.3), the coordinates relative to the decay point of the following three points are needed; the first measured point on the charged secondary and the conversion points of the two gamma rays. To study how measurement errors affect these relative coordinates, a sample of events which for various reasons were measured at least three times was obtained. Only events which were remeasured for reasons unrelated to the relative coordinates being studied were used in the sample. The sample contained 84 points each of which was measured at least three times. The root-mean-square deviation of each coordinate about its mean was calculated yielding 0.0294 cm for the X- and Y-, and 0.0617 cm for the Z-coordinates. The Z-coordinate is subject to more error because the Z-direction is perpendicular to the plane of the cameras. For use in the Monte Carlo calculations, measurement errors in the X- and Y-directions were assumed

to be normally distributed with mean 0 and standard deviation 0.0294 cm, while in the Z-direction, normally distributed with mean 0 and standard deviation 0.0617 cm. In both directions, the maximum allowed error was three standard deviations.

8. MULTIPLE SCATTERING PERTURBATION

Another important effect closely related to measurement errors is the multiple scattering of the charged secondary. The measurers were instructed to measure the first point on the charged secondary such that the following conditions were satisfied: the segment of track between the decay point and the first point on the charged secondary had to be straight, yet long enough to permit accurate determinations of the direction cosines. Due to multiple scattering, it was not always possible to do this, hence an addition to the Monte Carlo events to account for multiple scattering was made.

Multiple scattering is considered to be a perturbation of the secondary direction such that if the secondary really goes in the direction $\hat{S}_1$, it is measured as if it goes in the direction $\hat{S}_2$. The small angle included between the vectors $\hat{S}_1$ and $\hat{S}_2$ is called the multiple-scattering angle Θ. Θ is assumed to be normally distributed with mean 0 and standard deviation, σ, given by[19]

$$\sigma = \arctan (9.744 E\sqrt{X}/P^2)$$

where E and P are the energy and momentum of the charged secondary in MeV and MeV/c, X is the distance from the decay point to the first measured point on the charged secondary in centimeters, and σ is in radians. The azimuthal variation of $\hat{S}_2$ relative to $\hat{S}_1$ was chosen randomly. The maximum allowable multiple-scattering angle is called the multiple-scattering cutoff angle.

In order to guarantee that the Monte Carlo events, with their artificial measurement errors and multiple-scattering perturbations, simulate the real events as closely as possible, the best value to use for the multiple-scattering cuttoff angle was determined as follows.

As explained in Section III.B.3, the quantities that determine how well a two-gamma event fits $K_{\pi 2}$ kinematics are DEVCOP, ERFIT, and KINFIT, where KINFIT is the square root of the sum of the squares of DEVCOP and ERFIT. Of the measured events that pass $K_{\pi 2}$ kinematics, 98% are real $K_{\pi 2}$ decays. For this sample of events, the following quantities were calculated.

a. The average ERFIT.

b. The average KINFIT.

c. The root-mean-square DEVCOP.

d. The root-mean-square ERFIT.

e. The root-mean-square KINFIT.

These quantities were also calculated for the Monte Carlo $K_{\pi 2}$ decays and values of the multiple-scattering cutoff angle equal to 0°,

1°, 2°,...,10°. It was found that the best value to use for the multiple-scattering cuttoff angle was 5.74° ± 1°. An error of 1° here is equivalent to an error of 0.005 in $P(K_{\pi 2})$, the probability that a two-gamma $K_{\pi 2}$ will pass $K_{\pi 2}$ kinematics.

Figure 5 shows the distribution of KINFIT for the real $K_{\pi 2}$ decays and for the Monte Carlo $K_{\pi 2}$ decays. The experimental curve has been extrapolated beyond 8.5°, the cutoff for events which pass the $K_{\pi 2}$ kinematical test. Monte Carlo curves with values of multiple-scattering cutoff angle of 1° greater and 1° less than the actual value used have tails that lie on either side of the tail of the experimental curve. This means that the error of ±1° in the multiple-scattering cutoff angle is satisfactory.

9. DECAY IN FLIGHT PERTURBATION

The Monte Carlo programs contained as an input parameter, the K^+ momentum, allowing decays in flight to be simulated. The results will be discussed in Section IV.D.5.

B. Biases

The biases that occurred in the present experiment will be discussed now. The treatment of the biases will be discussed later.

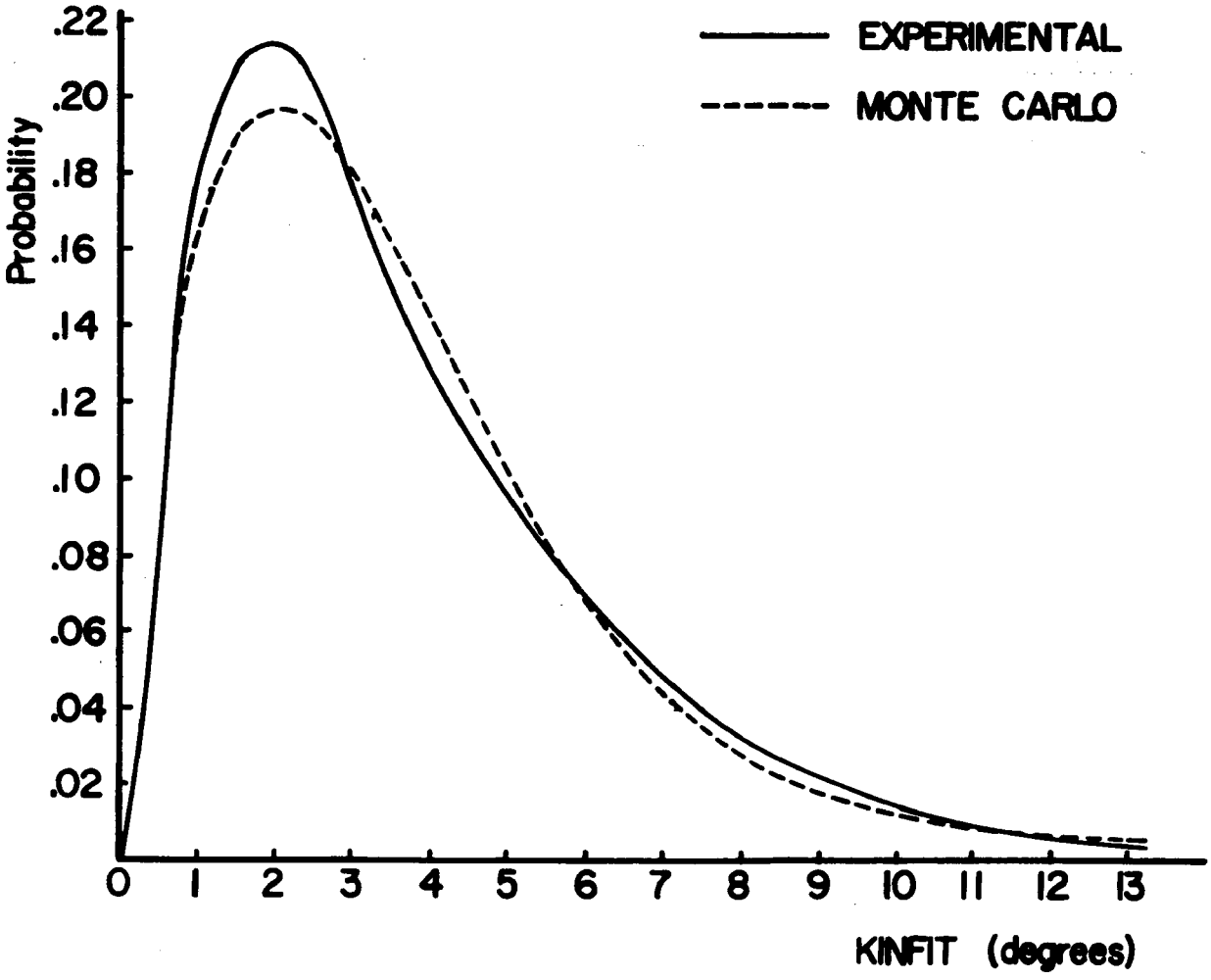


Figure 5. Curves showing how the distribution of KINFIT for the real $K_{\pi 2}$ events (experimental curve) compares with the distribution of KINFIT for the simulated $K_{\pi 2}$ events (Monte Carlo curve). Both curves are normalized giving total probabilities of 1.

1. GAMMA-RAY SCANNING BIASES

Scanning biases pertaining to the electron pairs created by gamma rays from π°'s can be divided into three groups.

a. Directional bias. There was considerable bias against dipped electron pairs, i.e., against electron pairs created by gamma rays coming toward or going away from the cameras.

b. Energy bias. There was some bias against gamma rays with energies between 20 MeV (the lowest possible gamma ray energy) and 70 MeV.

c. Gamma ray ambiguities. Following is a list of cases in which the identification of a gamma is not clear.

(1) Gamma rays that could belong to more than one K^{+} decay.

(2) Gamma rays that convert too close to the chamber walls allowing insufficient room for positive identification.

(3) Electron pairs that are hard to see because they are mixed up with other tracks.

(4) Good gamma rays that are not counted because the electron pairs are oddly shaped.

(5) Background junk counted as electron pairs.

(6) Confusion between gamma rays and bremsstrahlung from electrons in the chamber.

The individual biases listed above under (c) are small, but collectively they are significant.

2. SECONDARY SCANNING BIASES

It was mentioned previously, but will be repeated here for convenience, that the charged secondaries of the K^+ decays were classified into the following categories; e^+, N, SD, both N and SD, and OCT. e^+ means the secondary was called an e^+; N means the secondary underwent a nuclear interaction in the chamber; SD means the secondary stopped and decayed in the chamber; OCT means the secondary left the chamber with no nuclear interaction or indication of an electron. As mentioned earlier, the μ^+ secondary from π^+ decays at rest is too short to allow a reliable separation between stopping π and μ secondaries on the basis of π-μ decays.

With the above secondary classifications, the following scanning biases exist.

a. Secondary ambiguities. Secondaries can erroneously be placed in the wrong category. In addition, some secondaries are inherently ambiguous, i.e., it is impossible to decide in which category the secondary belongs. The most serious ambiguity is between SD and e^+.

b. Directional bias. Dipped secondaries have a tendency to be misclassified or ambiguous. For example, a very dipped π^+ secondary can appear to have more multiple scattering than it really has and be classified as an e^+.

c. Energy bias. Low-energy π^+ and μ^+ secondaries with ranges less than about 0.5 mm are very likely to be called e^+ sec-

ondaries. High-energy e^+ secondaries can leave the chamber without exhibiting the characteristic e^+ behavior, namely, large radiative energy loss or production of a cascade shower. They will be called OCT and hence misclassified.

3. BIASES INVOLVING COMPLETE DECAYS

The following biases can neither be called gamma-ray biases nor secondary biases.

a. τ decays with three charged secondaries can become confused with one or two gamma decays in which the gammas convert very close to the decay point and the secondary is fairly short.

b. There may be π^+ contamination in the K^+ beam, and some of the π^+ decays can become confused with K^+ decays.

c. Background junk in the chamber may simulate a decay, or a decay may be called background junk.

d. Some decays are simply missed.

e. Decays in flight may be called at rest and decays at rest may be called in flight.

C. Bias Reduction

Following is a discussion of the steps taken to reduce the previously mentioned biases as much as possible.

1. FIDUCIAL VOLUME FOR DECAY POINTS

The fiducial volume is defined as that region in the chamber containing all points which are at least 5 cm from every wall of the chamber. Only those K^+ decays which occurred inside this fiducial volume were used in the present experiment. This increases both the electron recognition efficiency and the gamma-ray conversion probability. It also helps to reduce π^+ contamination.

2. REDUCTION OF π^+ CONTAMINATION

Two steps were taken to further reduce the chance that a π^+ which enters the chamber with the beam, subsequently stopping and decaying, will be called a K^+. First, only those events which entered the chamber with a deviation from the beam direction of less than 20° in all four views as measured on the scanning projector were counted. This reduces the π^+ contamination because a π^+ has more chance than a K^+ of scattering in the moderator and also because those π^+'s coming from K^+'s decaying in flight before entering the chamber will deviate a certain amount from the beam direction. Second, the decays classified as zero-gamma electrons were not counted because of their possibility of being π^+ decays.

3. REJECTION OF CROWDED FRAMES

To reduce gamma-ray and secondary ambiguities, pictures having five or more K^+ decays on them were not counted.

4. GAMMA-RAY POTENTIAL PATH REQUIREMENT

An electron pair from a gamma ray had to have at least 2 cm of potential path in the chamber to allow sufficient room for positive identification.

5. CLOSE CONVERTING GAMMA RAYS

Gamma rays having conversion distances less than 3 mm from the K^+ decay point were counted in order to distinguish the decay from a $K_{\mu 2}$ which has no gammas. However, any decay having such a gamma was automatically excluded from the $K_{\pi 2}$ kinematical test because of the difficulty of obtaining accurate direction cosines.

6. GAMMA-RAY DIP-ANGLE SELECTION RULE

Figure 6 shows a histogram of the Z-direction cosines of all the troublesome gamma rays found in the fine scanning (the Z-direction is perpendicular to the plane of the cameras). These gamma rays are all the ones that the original scanners either missed or assigned to the wrong origin. They also include those that were labeled ambiguous by the physicists. The χ^2 probability that the Z-direction cosines are uniformly distributed is less than 0.1. However, in the range from -0.8 to +0.8, the same χ^2 probability is 0.71.

Figure 7 shows a histogram of the Z-direction cosines of all the gamma rays on about 10% of the film, excluding gamma rays with potential path less than 2 cm and those with conversion distances less than 3 mm.

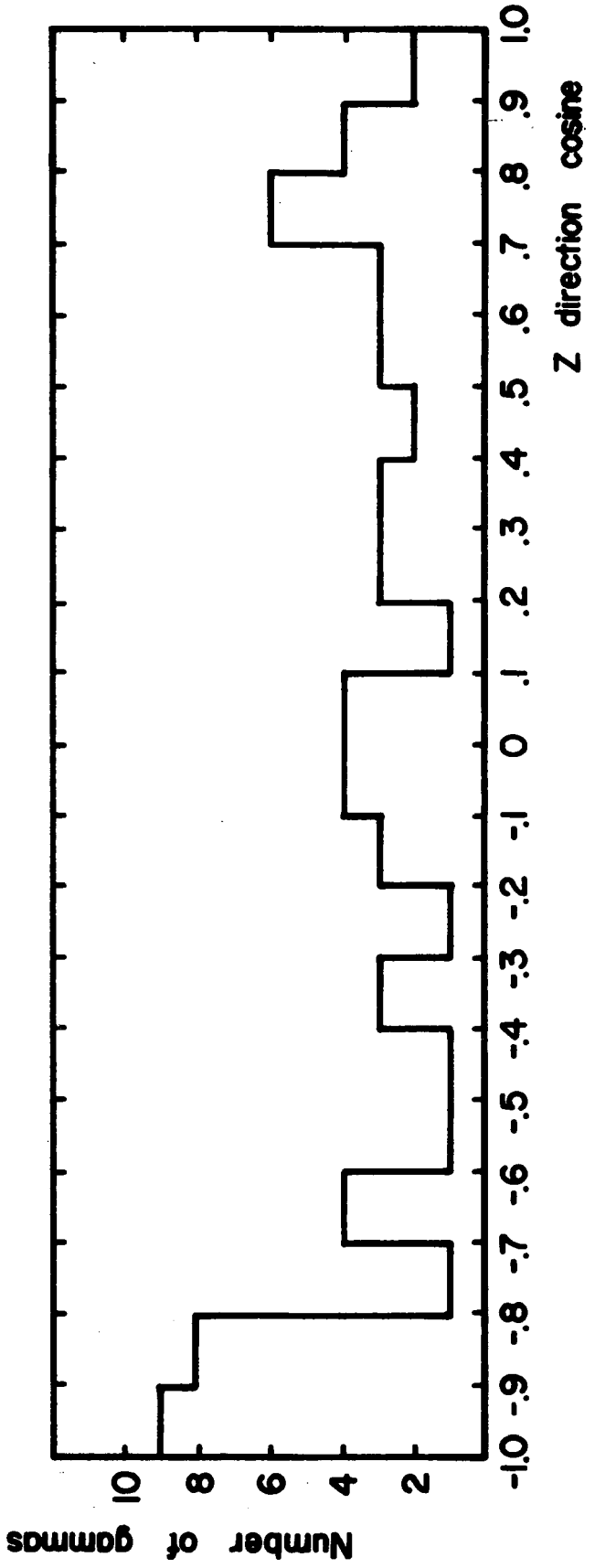


Figure 6. The distribution of Z-direction cosines for 66 gamma rays that were missed by the scanners and measurers.

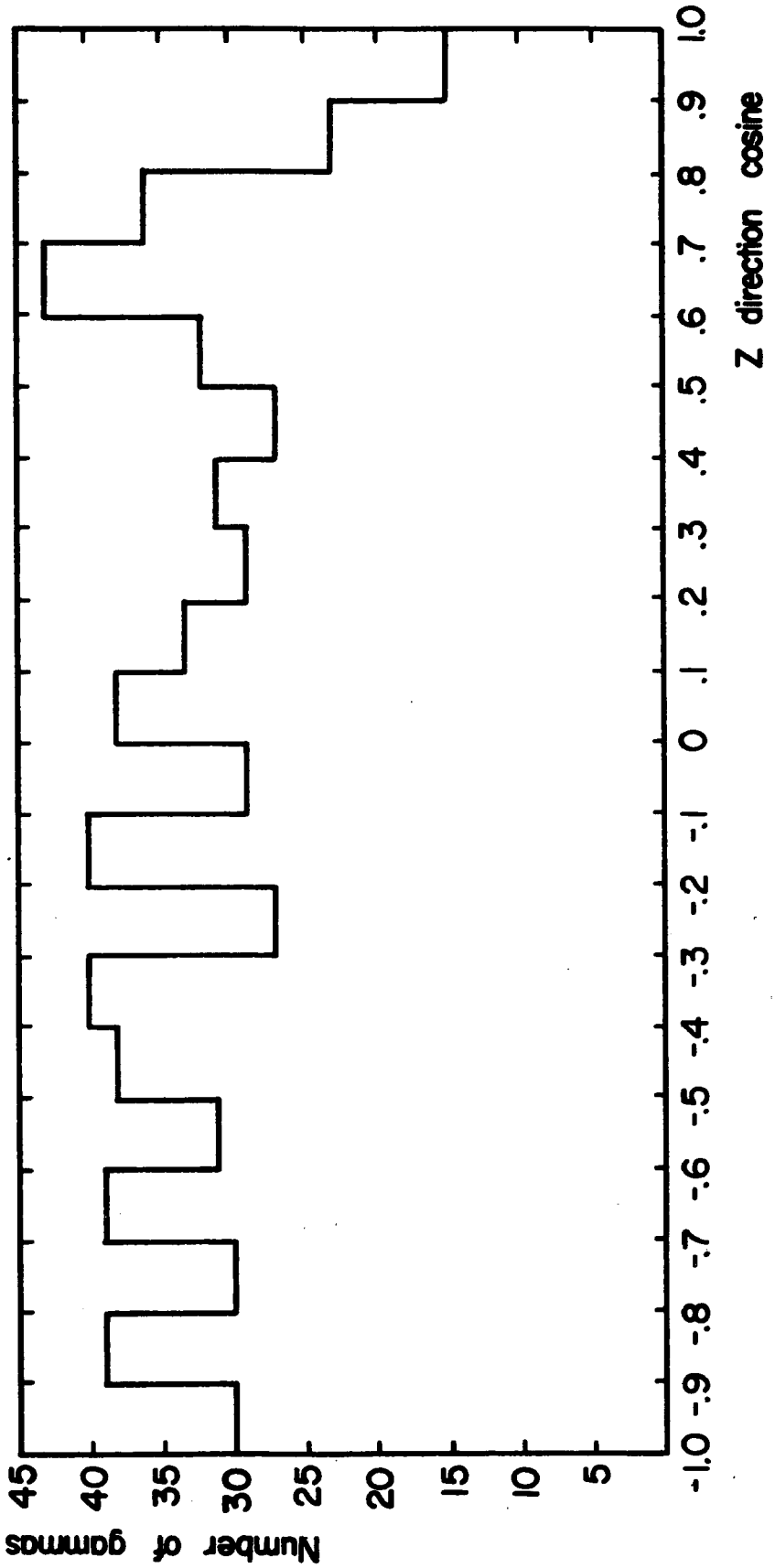


Figure 7. The distribution of Z-direction cosines for 650 gamma rays.

The deficiency in the region from 0.8 to 1.0 is due to the fact that the beam was slightly off center, causing the decay points to be shifted slightly toward the +Z-direction, and allowing less xenon and hence less conversion probability for those gammas going in the +Z-direction. In the region from -0.8 to +0.8, the χ^2 probability that the Z-direction cosines are uniformly distributed is 0.69.

Comparing Figures 6 and 7, one can see that in the regions -1.0 to -0.8 and +0.8 to +1.0, the fraction of ambiguous gamma rays is higher than in the region -0.8 to +0.8. It was therefore decided that all gamma rays having Z-direction cosines greater than 0.8 in absolute magnitude would be discarded. This meant that about 35% of the ambiguous gamma rays were eliminated, at the expense of only about 15% of all gamma rays. The main advantage is that in the range -0.8 to +0.8 for gamma-ray Z-direction cosines, the scanning efficiency, while not 100%, is at least isotropic. This fact alone turned out to be very helpful in the evaluation of overall gamma-ray scanning bias.

7. SECONDARY DIP-ANGLE SELECTION RULE

Figure 8 is a histogram showing the distribution of the Z-direction cosines of all the troublesome secondaries found in the fine scanning. The peaking at the ends is more striking for secondaries than it is for gamma rays. It was decided that all K^+ decays with charged secondaries having Z-direction cosines greater than 0.9 in magnitude would be discarded. This meant that 35% of the ambiguous

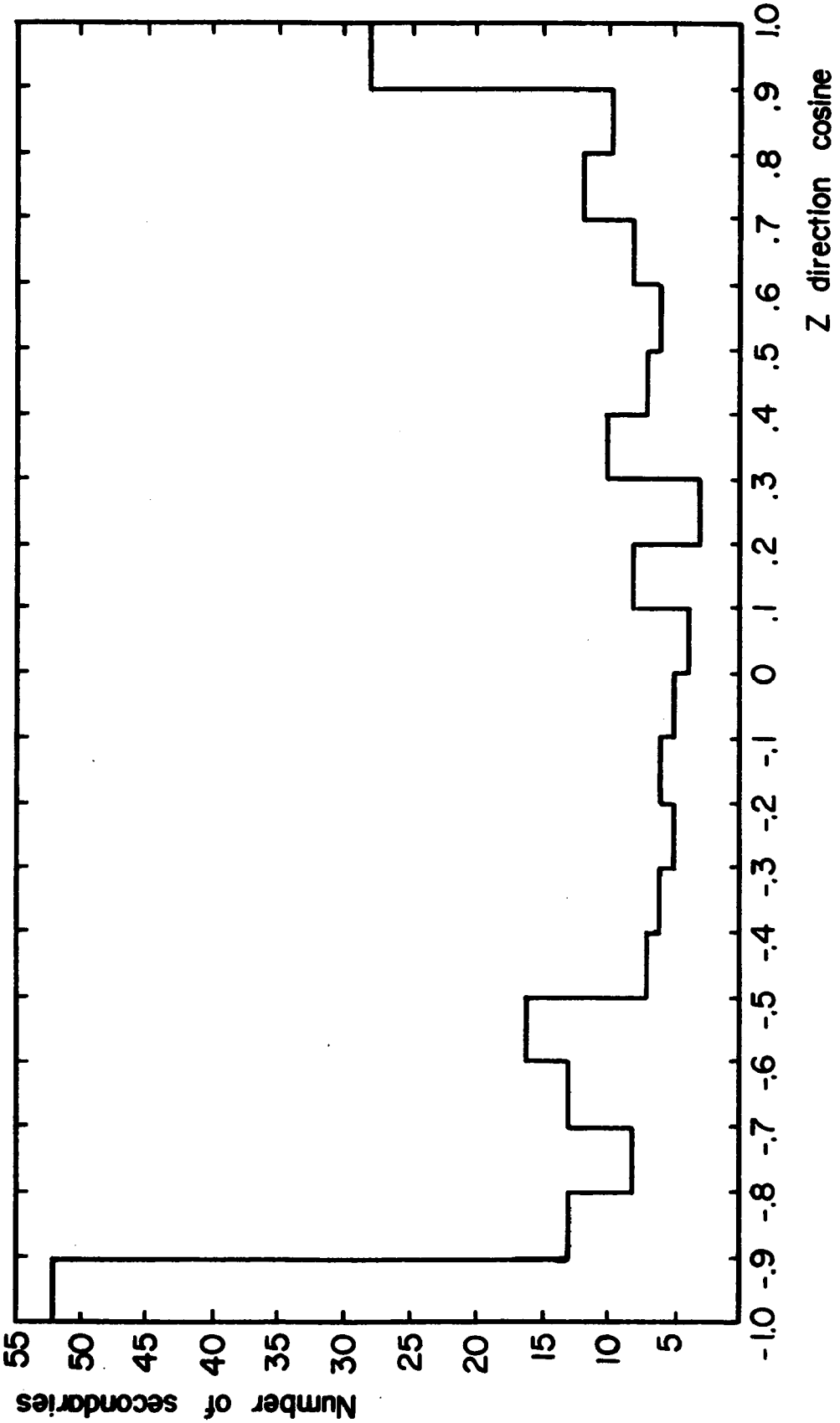


Figure 8. The distribution of Z-direction cosines for all the ambiguous secondaries.

events, but only 10% of all the events were lost. It also meant that the electron recognition efficiency was raised.

8. SECONDARY RECLASSIFICATION

Because of the difficulties involved in separating the charged secondaries into the various categories described previously, it was decided to use only two categories to separate the secondaries; electron and nonelectron. The disadvantage is that some information is lost because secondaries formerly classified as nuclear, for example, were known to be π^+'s, whereas they are now reclassified as nonelectron and hence could be π's or μ's. This is not a serious loss since only about 3% of all secondaries were classified as nuclear. The advantage is that the analysis is very much simplified and freed from possible sources of error that would arise from calculating, for example, the probability that a μ^+ from a $K_{\mu 3}$ will stop and decay in the chamber. The number of ambiguous secondaries in the final data sample was about 37, divided equally between the electron and nonelectron categories.

D. Bias Compensation

1. CORRECTING FOR LOW-ENERGY GAMMA RAYS

The histogram in Figure 9 shows the energy distribution of the lower energy gamma ray for the measured two-gamma $K_{\pi 2}$'s. The curve shows the energy distribution for the Monte Carlo $K_{\pi 2}$'s. It was

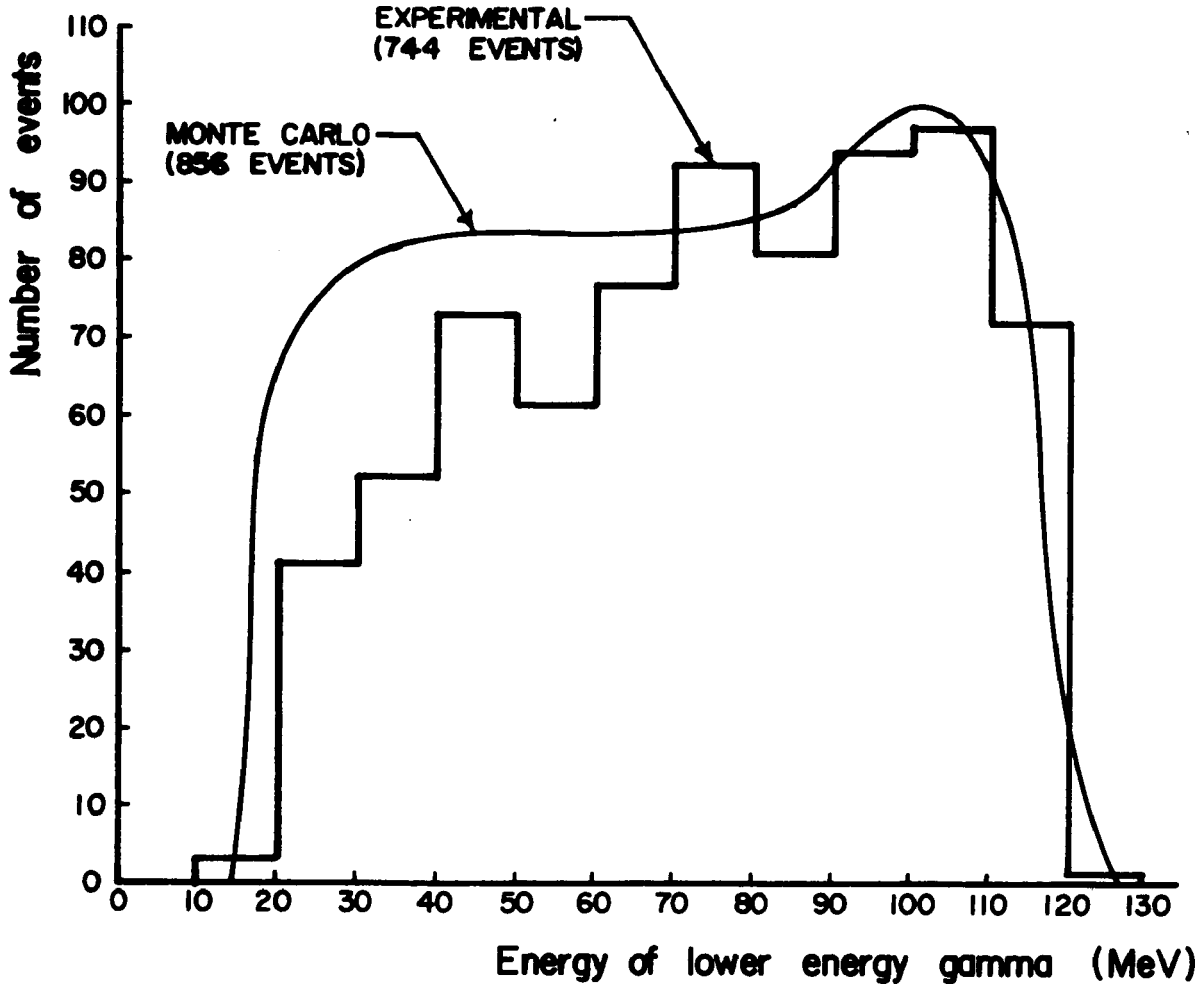


Figure 9. Experimental and Monte Carlo energy distribution of the lower energy gamma ray for $K_{\pi 2}$ decays.

assumed that there was no bias against gamma rays with energy greater than 70 MeV. Hence the Monte Carlo curve was normalized by fitting it to the histogram above 70 MeV by the least squares method. Below 70 MeV the histogram falls off with energy relative to the Monte Carlo curve. This is due to scanning bias against low-energy gamma rays. The Monte Carlo programs were modified to account for this low-energy bias.

2. CORRECTING FOR OTHER MISSED GAMMA RAYS

In addition to low-energy bias, the Monte Carlo programs were corrected for overall gamma-ray scanning biases. It was estimated that aside from low-energy and dipped gammas, the physicists' scanning efficiency was (98 ± 1)%, while the professional scanners' efficiency was (95 ± 1)%. These estimates were based on the observed 1-gamma/2-gamma ratio for $K_{\pi 2}$ and $K_{\mu 3}$ events which was 1.68 ± 0.07. The Monte Carlo ratio based on the above estimates was 1.62 ± 0.05. The observed 3-gamma/4-gamma ratio was 2.6 ± 0.6 as compared to the Monte Carlo ratio of 2.44.

3. CORRECTING FOR LOW-ENERGY PIONS FROM τ' DECAYS

It was estimated that about 17% of the pions from τ' decays have momenta less than 34 MeV/c and hence ranges less than 1 mm in xenon. From observing π-μ-e decays in which the μ has a constant range of 1.3 mm, it was known that the efficiency for detecting the μ, even

knowing it was there somewhere, was less than 50%. It was therefore important to know how many short pions from τ' decays were missed in scanning, causing the τ' decays to be called K_{e3}'s.

The physicists carefully scanned 142 π^+'s from τ decays and found 10 that would be called electrons if it were not known that they came from τ decays and hence had to be π^+'s. The statistical fluctuation in these 10 events is about 3.1, therefore it was estimated that $(7 \pm 2)\%$ of the 0-, 1-, and 2-gamma τ' decays were indistinguishable from K_{e3} decays. The π^+-momentum spectrum for τ'[20] was compared to the π^+-momentum spectrum for τ[21] for low pion momenta. The difference was certainly not enough to affect the above estimate of $(7 \pm 2)\%$.

4. CORRECTING FOR LOW-ENERGY MUONS FROM $K_{\mu 3}$ DECAYS

From the $K_{\mu 3}$ muon-energy spectrum, it was estimated that approximately 1% of the muons from $K_{\mu 3}$ decays have momenta less than 28 MeV/c and hence ranges less than 1 mm in xenon. The fraction of $K_{\mu 3}$ decays that were indistinguishable from K_{e3} decays due to short muons was estimated to be $(0.5 \pm 0.5)\%$.

5. CORRECTING FOR DECAYS IN FLIGHT

As will be shown later, the $K_{\pi 2}/K_{\mu 3}$ branching ratio is very sensitive to the fraction of $K_{\pi 2}$'s that fail the $K_{\pi 2}$ kinematical test. It is therefore very important to calculate as accurately as possible the

contribution that decays in flight make to this $K_{\pi 2}$ failure rate.

All K^+ decays in flight that were detected in scanning were discarded. However, a K^+ decaying in flight with a short residual range (less than about 3 cm) cannot be distinguished in scanning from a decay at rest. Figure 10 summarizes the kinematics of a K^+ stopping in xenon, and is based on the range-energy-residual time relationships calculated by Professor George H. Trilling of the Lawrence Radiation Laboratory, using the Bethe-Bloch formula and parameters given by Sternheimer[22] and Walske.[23] The K^+ momentum is shown in Figure 10 to illustrate the fact that it is appreciable even for small residual ranges.

Suppose x is the residual range cutoff, i.e., if the kaons decay with a residual range greater than x, they are detectable in scanning as decays in flight and discarded. If the residual range is less than x, the decays are not detectable as decays in flight and are kept. By assuming a value for x, one can calculate $P(K_{\pi 2})$, the probability that a $K_{\pi 2}$ decay will pass $K_{\pi 2}$ kinematics, by numerically evaluating the following integral:

$$P(K_{\pi 2}) = \int_0^x P_1(y)P_2(y)dy$$

where $P_1(y)dy$ is the probability that a kaon will decay with residual range between y and y + dy, and $P_2(y)$ is the probability that a $K_{\pi 2}$ decay with residual range y will pass $K_{\pi 2}$ kinematics. $P_1(y)$ and $P_2(y)$

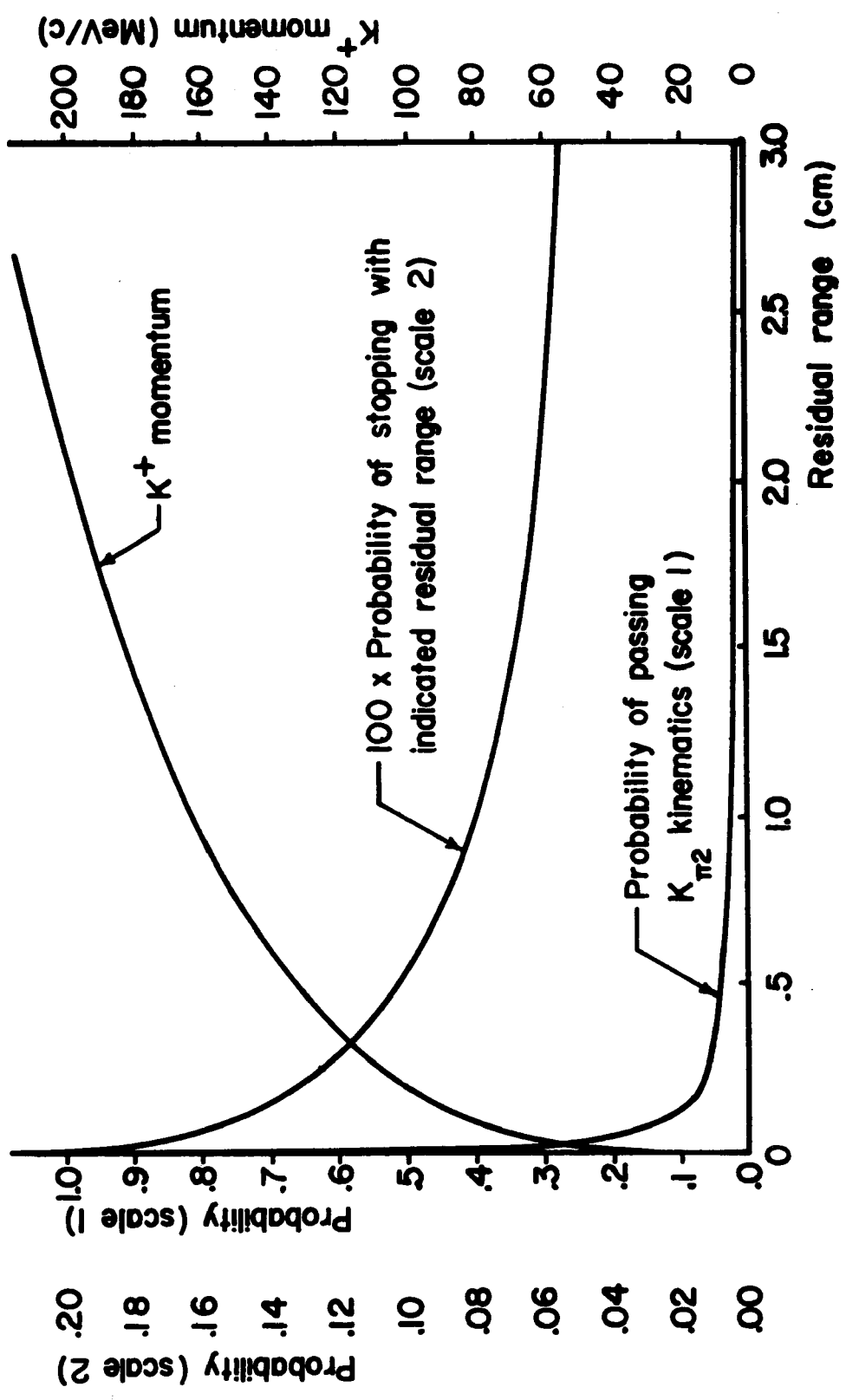


Figure 10. Kinematics of a K^+ stopping in xenon.

are shown in Figure 10. The variation of $P(K_{\pi 2})$ as a function of x is shown in Figure 11.

The average range of the kaons is about 14 cm, which means that the average time it takes the kaons to come to rest is about 8.92×10^{-10} sec. Using 1.22×10^{-8} sec as the K^+ lifetime, the probability that a K^+ will decay in flight is

$$1 - \exp(-8.92 \times 10^{-10}/1.22 \times 10^{-8}) = 0.0705$$

Thus about 7% of the decays are in flight. In the final sample of 895 two-gamma nonelectron events, 54 were called in flight in scanning, which amounts to $(6 \pm 1)\%$, where the error is due to the statistical fluctuation of 54 out of 895 events. The fraction of undetected decays in flight is therefore about $(1 \pm 1)\%$. This corresponds to a residual range cutoff of about 1.5 ± 1.5 cm, which from Figure 11, gives $P(K_{\pi 2}) = 0.925$. The upper limit of 3.0 cm for the residual range cutoff was verified by the physicists who scanned about 60 K^+ decays at rest, estimating the residual range cutoff for each. Combining the error due to the present analysis with the error due to the simulation of real $K_{\pi 2}$'s by Monte Carlo $K_{\pi 2}$'s gives the final value

$$P(K_{\pi 2}) = 0.925 \pm 0.008$$

6. ELECTRON RECOGNITION EFFICIENCY

The probability of recognizing an electron secondary from a K_{e3} decay depends on the electron energy and the potential path available

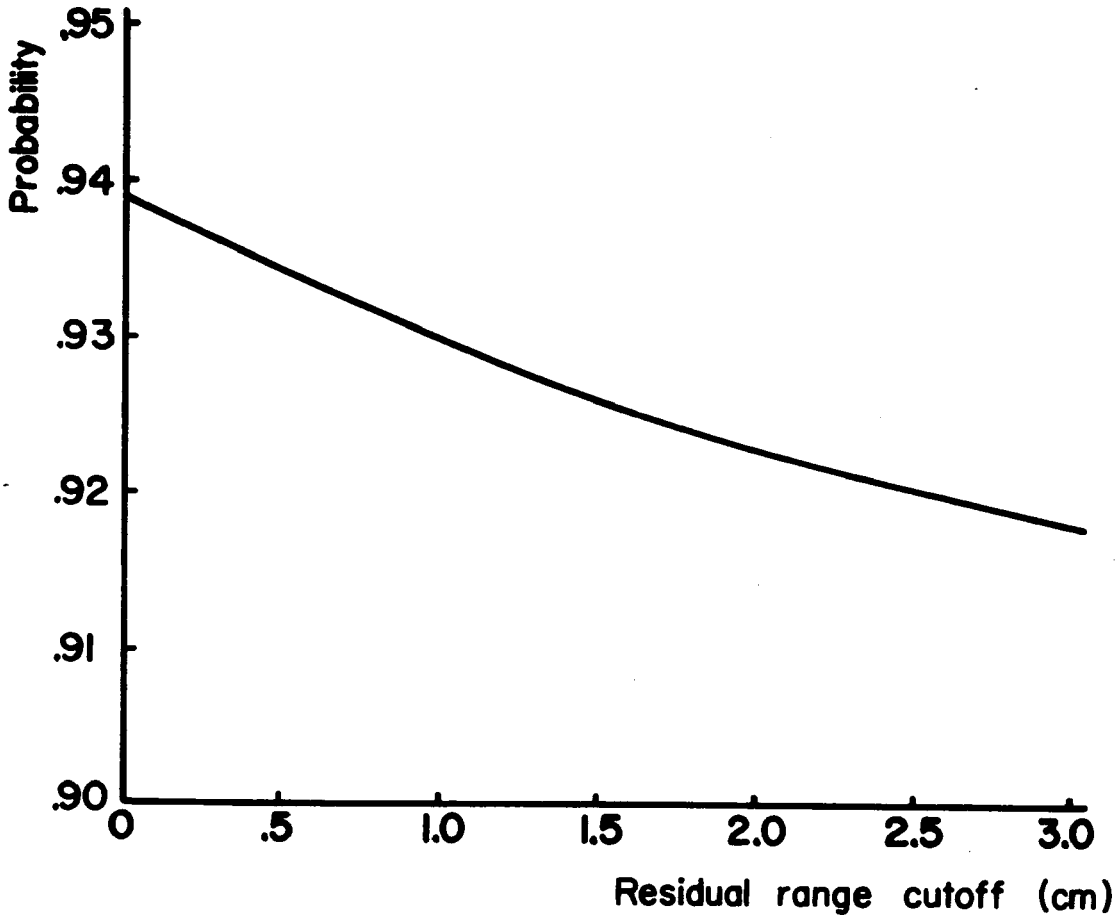


Figure 11. Probability of a two-gamma $K_{\pi 2}$ passing $K_{\pi 2}$ kinematics as a function of the residual range cutoff.

to the electron. This probability must be known in order to make corrections for those electron secondaries that left the chamber without being recognized. This section will describe how the electron recognition efficiency was obtained from the data.

Each electron secondary in the final sample of 436 one- and two-gamma K_{e3}'s was scanned by a physicist who measured the minimum distance in which the electron could be recognized, hereafter called the electron recognition distance. Zero-gamma K_{e3}'s were excluded because of the possibility of confusing them with beam pions. The reader is reminded here that the final sample excludes all decays occurring less than 5 cm from the chamber boundaries. It also excludes all dipped electron secondaries, i.e., those having Z-direction cosines greater than 0.9 in magnitude.

If r is the electron recognition distance, the number n(x,y) is defined as the number of electrons having at least y cm of potential path and having $x \leq r \leq y$. Using different values for x and y, the numbers n(x,y), obtainable directly from the data, were used to calculate P(s), the probability of recognizing an electron within s cm from the decay point. P(s) is shown in Figure 12.

The electron recognition efficiency, C_e, was obtained by numerically evaluating the integral

$$C_e = \int_{s_{min}}^{s_{max}} P(s)P_1(s)ds = 0.974 \pm 0.010$$

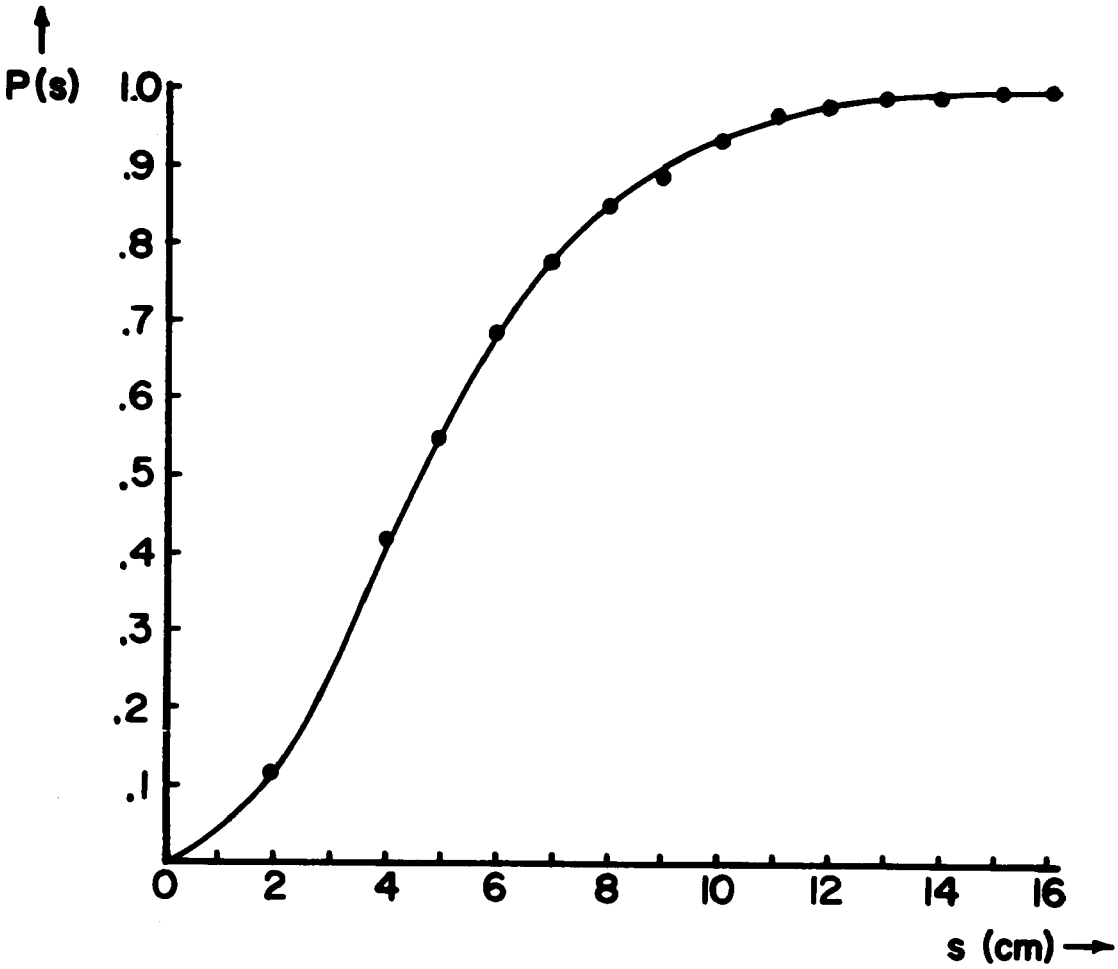


Figure 12. P(s), the probability that an electron secondary with potential path s will be recognized.

where P(s) is defined above, $P_1(s)ds$ is the probability that the electron from a one- or two-gamma K_{e3} will have potential path between s and s + ds, and s_{max} and s_{min} are the maximum and minimum values of potential path available to the electrons (s_{min} = 5 cm). $P_1(s)ds$ was obtained from the K_{e3} Monte Carlo program.

E. Calculating the Branching Ratios

The important numbers used in this section are summarized in Tables III and IV, pp. 57 and 58.

1. THE NUMBER OF τ DECAYS IN THE FIDUCIAL VOLUME

Since the τ decay mode is recognized in scanning by its three charged secondaries, no measurements of τ decays were made. Consequently, it was necessary to calculate the number of τ decays that occurred in the fiducial volume. The total number of τ decays found by the scanners is 797. This number, corrected for systematic errors according to the results of the physicists' scanning, is 790 ± 32. The quoted error of 32 is mostly statistical, but includes error due to ambiguous events. From those events that were measured to give an unbiased distribution of decay points in the chamber, it is known that (76.1 ± 1.2)% of the τ decays occurred inside the fiducial volume. Finally, discarding 10% of the τ decays because of the secondary dip-angle selection rule, the number of τ decays in the fiducial volume is 540 ± 23.

2. THE NUMBER OF ZERO-GAMMA EVENTS IN THE FIDUCIAL VOLUME

Not all of the zero-gamma events were measured either, hence it was also necessary to calculate the number of zero-gamma events in the fiducial volume. This number is 6919 ± 139. The error is mostly statistical, but includes errors due to ambiguous events and due to the error in the fraction of zero-gamma events occurring in the fiducial volume, (73.7 ± 1.4)%.

3. THE NUMBER OF ZERO-GAMMA RECOGNIZED K_{e3} DECAYS

Because zero-gamma events having secondaries identified as electrons were not counted in order to reduce π^+ contamination, the number of recognized zero-gamma K_{e3}'s was calculated by means of the K_{e3} Monte Carlo program. The fraction of K_{e3}'s that have no observed gamma rays in the chamber is 0.106 ± 0.010. The total number of one- and two-gamma recognized K_{e3}'s is 436 ± 23. Hence the number of recognized zero-gamma K_{e3}'s is 52 ± 6.

Having calculated the number of τ decays and the number of zero-gamma decays in the fiducial volume, the total number of decays can be calculated, giving 10513 ± 141.

4. THE τ BRANCHING RATIO

Knowing the number of τ decays, 540 ± 23, and the total number of decays, 10513 ± 141, the τ branching ratio can be calculated. The result is 0.051 ± 0.002.

5. THE τ' BRANCHING RATIO

The number of K^+ decays having three or four gamma rays, after all selection criteria were applied, is 108 ± 10. From the τ' Monte Carlo program, this number is (57.0 ± 1.8)% of all the τ' decays. Hence the total number of τ' decays is 189 ± 19 and the τ' branching ratio is 0.018 ± 0.002.

6. THE K_{e3} BRANCHING RATIO

The number of one- and two-gamma decays with secondaries identified as electrons and satisfying all selection criteria is 436 ± 23. Since (7 ± 2)% of the one- and two-gamma τ' decays and (0.5 ± 0.5)% of the one- and two-gamma $K_{\mu 3}$ decays were called K_{e3} decays because of their low-energy charged secondaries, the 436 ± 23 includes 6 ± 1 τ' decays and 1 ± 1 $K_{\mu 3}$ decays. Hence the actual number of recognized K_{e3} decays is 429 ± 23. The error would be ± 20 due to statistics alone, but the ambiguous and questionable events raise the error to ± 23.

According to the electron recognition efficiency (Section IV.D.6), the number of recognized K_{e3}'s, 429 ± 23, is only (97.4 ± 1.0)% of the actual number of K_{e3}'s. The electrons from the remaining 2.6% left the chamber without being recognized. Hence the real number of one- and two-gamma K_{e3}'s, both recognized and unrecognized is 440 ± 24.

From the K_{e3} Monte Carlo program, the number of one- and two-gamma K_{e3}'s, 440 ± 24, is (89.4 ± 1.0)% of all the K_{e3} decays. Hence the

total number of K_{e3}'s, satisfying all selection criteria, is 493 ± 28, giving the K_{e3} branching ratio of 0.047 ± 0.003.

7. THE $K_{\mu 3}$ BRANCHING RATIO

The total number of two-gamma events with secondaries identified as pions or muons is 940. Subtracting the number of two-gamma unrecognized K_{e3}'s (4) and the number of two-gamma τ' decays (50) leaves 886 ± 6 as the sum of the two-gamma $K_{\mu 3}$ and $K_{\pi 2}$ modes only. The error is due only to the errors in the subtracted events. Similarly, the sum of the two-gamma $K_{\mu 3}$ and $K_{\pi 2}$ modes which pass the $K_{\pi 2}$ kinematical test is 734 ± 11 where the error is due mainly to the statistical fluctuation of 734 out of 886 events.

From the $K_{\pi 2}$ and $K_{\mu 3}$ Monte Carlo programs, the probabilities of a two-gamma $K_{\pi 2}$ and a two-gamma $K_{\mu 3}$ passing the $K_{\pi 2}$ kinematical test are 0.925 ± 0.008 and 0.094 ± 0.002, respectively. Let $B(K_{\pi 2})$ = the $K_{\pi 2}$ branching ratio, $B(K_{\mu 3})$ = the $K_{\mu 3}$ branching ratio, and $R = B(K_{\pi 2})/B(K_{\mu 3})$. Then $(R/R+1)(0.925 \pm 0.008)$ is the probability that if K_{e3} and τ' decays are excluded, a two-gamma event that passes $K_{\pi 2}$ kinematics is a $K_{\pi 2}$. $(1/R+1)(0.094 \pm 0.002)$ is the corresponding probability for $K_{\mu 3}$ decays. Therefore,

$$\frac{R}{R+1}(0.925 \pm 0.008) + \frac{1}{R+1}(0.094 \pm 0.002) = (734 \pm 11)/(886 \pm 6)$$

Solving for R gives $R = 7.6 \pm 1.3$.

The number of one-gamma decays with nonelectron secondaries is 1618 ± 37. Subtracting the number of one-gamma unrecognized electron events, 7 ± 3, and the number of one-gamma τ' events, 24 ± 4, leaves 1487 ± 37 which is the sum of the one-gamma $K_{\pi 2}$ and $K_{\mu 3}$ events and is (14.1 ± 0.4)% of the total number of events. From the $K_{\pi 2}$ and $K_{\mu 3}$ Monte Carlo programs, the probabilities that a $K_{\pi 2}$ and a $K_{\mu 3}$ will have only one gamma convert and be observed in the chamber are 0.551 ± 0.004 and 0.552 ± 0.005, respectively. Hence

$$B(K_{\pi 2})(0.551 \pm 0.004) + B(K_{\mu 3})(0.552 \pm 0.005) = 0.141 \pm 0.004$$

Knowing $R = B(K_{\pi 2})/B(K_{\mu 3}) = 7.6 \pm 1.3$, one can solve for $B(K_{\mu 3})$ and obtain

$$B(K_{\mu 3}) = 0.030 \pm 0.005$$

8. THE $K_{\pi 2}$ BRANCHING RATIO

The $K_{\pi 2}$ branching ratio could be obtained from $B(K_{\mu 3})$ and the ratio $R = B(K_{\pi 2})/B(K_{\mu 3})$. However, it is more accurate to first calculate $S = B(K_{\pi 2}) + B(K_{\mu 3})$ and obtain $B(K_{\pi 2})$ from $B(K_{\pi 2}) = S - B(K_{\mu 3})$.

The number of one- and two-gamma $K_{\pi 2}$ and $K_{\mu 3}$ events is 2372 ± 45. Adding the number of zero-gamma $K_{\pi 2}$ and $K_{\mu 3}$ events, obtained from the Monte Carlo programs, gives a total of 2666 ± 78 events which are pure $K_{\pi 2}$ and $K_{\mu 3}$ events. Hence

$$S = B(K_{\pi 2}) + B(K_{\mu 3}) = 0.254 \pm 0.007$$

from which

$$B(K_{\pi 2}) = 0.224 \pm 0.008$$

9. THE $K_{\mu 2}$ BRANCHING RATIO

The most accurate way to calculate the $K_{\mu 2}$ branching ratio is to subtract all of the previously obtained branching ratios from 1, giving 0.630 ± 0.008.

V. RESULTS

A. Numbers Needed to Calculate the Branching Ratios

Tables III and IV summarize the definitions and values of the complete set of quantities that were used to calculate the branching ratios, complete in the sense that the branching ratios follow from these numbers alone.

B. Summary of Results

Table I, p. 2, summarizes the results of the present experiment, along with the results of previous experiments. Table V compares the experimental results with the theoretical predictions that were discussed in Section I.B.

C. Discussion

1. SENSITIVITY OF THE $K_{\pi 2}/K_{\mu 3}$ BRANCHING RATIO

As mentioned earlier, R, the $K_{\pi 2}/K_{\mu 3}$ branching ratio, is very sensitive to $P(K_{\pi 2})$, the probability that a two-gamma $K_{\pi 2}$ will pass the $K_{\pi 2}$ kinematical test. The equation used to calculate R was (see Section IV.E.7)

$$\frac{R}{R+1} P(K_{\pi 2}) + \frac{1}{R+1} P(K_{\mu 3}) = F$$

TABLE III

THE COMPLETE SET OF QUANTITIES USED TO CALCULATE THE BRANCHING RATIOS

Symbol	Definition
N_1	Number of decays having two or three charged secondaries.
N_2	Number of decays having three or four gamma rays seen in the chamber.
N_3	Number of decays having an electron secondary, and one or two electron pairs from gamma rays seen.
N_4	Number of events having a nonelectron secondary, exactly two measurable electron pairs,[a] and passing $K_{\pi 2}$ kinematics.
N_5	Number of events having a nonelectron secondary, exactly two measurable electron pairs, and failing $K_{\pi 2}$ kinematics.
N_6	Number of events having a nonelectron secondary, and no electron pairs.
N_7	Number of events having a nonelectron secondary but are not included in N_4, N_5, or N_6.
N	Total number of events.
C_e	Probability that an electron secondary will be recognized.
$C(K_i,j)$	Probability that in the decay mode K_i,j gammas will convert and be seen in the chamber.
$P(K_i)$	Probability that if the decay mode K_i has two measurable gammas, it will pass $K_{\pi 2}$ kinematics.
$Q(\tau')$, $Q(K_{\mu 3})$	Probability that the secondaries from τ' and $K_{\mu 3}$ decays are called electrons.

[a]A measurable electron pair is one which occurs at least 3 mm from the decay point.

TABLE IV

VALUES OF THE QUANTITIES DEFINED IN TABLE III

Symbol	Value	Symbol	Value
N_1	540 ± 23	$C(K_{\pi 2},0)$	0.108 ± 0.010
N_2	108 ± 10	$C(K_{\pi 2},1)$	0.551 ± 0.004
N_3	436 ± 23	$C(K_{\pi 2},2)$	0.340 ± 0.010
N_4	735 ± 26	$C(K_{\mu 3},0)$	0.113 ± 0.010
N_5	205 ± 14	$C(K_{\mu 3},1)$	0.552 ± 0.005
N_6	6919 ± 139	$C(K_{\mu 3},2)$	0.335 ± 0.011
N_7	1518 ± 37	$C(K_{e3},0)$	0.106 ± 0.010
N	10,513 ± 141	$C(K_{e3},1)$	0.556 ± 0.005
C_e	0.974 ± 0.010	$C(K_{e3},2)$	0.338 ± 0.011
$P(K_{\pi 2})$	0.925 ± 0.008	$C(\tau', 0)$	0.007 ± 0.002
$P(K_{\mu 3})$	0.094 ± 0.002	$C(\tau', 1)$	0.138 ± 0.014
$P(K_{e3})$	0.075 ± 0.002	$C(\tau', 2)$	0.285 ± 0.004
$P(\tau')$	0.013 ± 0.001	$C(\tau',3\&4)$	0.570 ± 0.018
$Q(\tau')$	0.070 ± 0.020		
$Q(K_{\mu 3})$	0.005 ± 0.005		

TABLE V

COMPARISON OF THE PRESENT EXPERIMENTAL RESULTS
WITH SOME THEORETICAL PREDICTIONS

Decay Ratio	Experimental Ratio	Theoretical Ratio
$\frac{K^+ \to \mu^+ + \pi^\circ + \nu}{K^+ \to e^+ + \pi^\circ + \nu}$	0.63 ± 0.10	0.64[a], 0.69[a], $0.651 + 0.126(f_-/f_+) + 0.0189(f_-/f_+)^2$[b]
$\frac{K^+ \to \pi^+ + \pi^\circ + \pi^\circ}{K^+ \to \pi^+ + \pi^+ + \pi^-}$	0.35 ± 0.04	0.325[c]
$\frac{K^+ \to \mu^+ + \nu}{K^+ \to \text{all modes}}$	0.630 ± 0.008	0.677 ± 0.011[d]

[a]See Ref. 7.
[b]See Ref. 6.
[c]Assuming the $\Delta T = 1/2$ rule is valid.
[d]See Ref. 12.

where F is the fraction of the sample of pure $K_{\pi 2}$ and $K_{\mu 3}$ decays that passes the $K_{\pi 2}$ kinematical test. Solving for R gives

$$R = \frac{F-P(K_{\mu 3})}{P(K_{\pi 2})-F}$$

The sensitivity comes from the denominator because the values of $P(K_{\pi 2})$ and F are not far apart. In fact,

$$P(K_{\pi 2}) = 0.925 \pm 0.008$$

and

$$F = 0.829 \pm 0.014$$

Subtracting,

$$P(K_{\pi 2})-F = 0.096 \pm 0.016$$

A major contribution to the error in $P(K_{\pi 2})-F$ comes from the statistical error in F, which is only about 1.8% of F. However, the error in $P(K_{\pi 2})-F$ is about 17%. This makes the error in the $K_{\mu 3}$ branching ratio about 15% and hence the error in the $K_{\mu 3}/K_{e3}$ branching ratio about 16%. Furthermore, a systematic error of 1% in determining $P(K_{\pi 2})$ reflects itself as a 10% systematic error in the $K_{\mu 3}$ and $K_{\mu 3}/K_{e3}$ branching ratios. For this reason, a large amount of effort has been made to reduce any systematic error in $P(K_{\pi 2})$ as much as possible.

2. COMPARING PAST AND PRESENT EXPERIMENTAL RESULTS

The past and present experimental results are summarized in Table I, p. 2. One can see that the present experimental results support fairly well the results of Roe et al.[4] with the exception of the $K_{\pi 2}$ and $K_{\mu 3}$ branching ratios, in which cases the present experiment is more in agreement with the emulsion results.[1-3] However, the sums of the $K_{\pi 2}$ and $K_{\mu 3}$ branching ratios for the present experiment and for the experiment of Roe et al. are in fairly good agreement. For the present experiment,

$$B(K_{\pi 2}) + B(K_{\mu 3}) = 0.254 \pm 0.007$$

while for Roe et al.,

$$B(K_{\pi 2}) + B(K_{\mu 3}) = 0.234 \pm 0.011$$

Therefore the only major disagreement between the present experiment and that of Roe et al. is in the $K_{\pi 2}/K_{\mu 3}$ branching ratio. For the present experiment,

$$B(K_{\pi 2})/B(K_{\mu 3}) = 7.6 \pm 1.3$$

while for Roe et al.,

$$B(K_{\pi 2})/B(K_{\mu 3}) = 3.9 \pm 0.5$$

It is believed that the disagreement is due to a systematic error in the Roe experiment in the calculation of $P(K_{\pi 2})$, the probability that

a $K_{\pi 2}$ will pass the $K_{\pi 2}$ kinematical test. In the present experiment, $P(K_{\pi 2})$ was calculated very carefully, simulating real $K_{\pi 2}$ decays by Monte Carlo decays.

Table I shows that the present experiment does not agree with the emulsion experiments in the $K_{\mu 2}$ branching ratio.

3. COMPARING EXPERIMENTAL AND PREDICTED RESULTS

Table V compares the experimental and predicted results. The reader will recall that the predicted value of the $K_{\mu 3}/K_{e3}$ branching ratio was determined by the ratio of the form factors, f_-/f_+, according to [6]

$$R = \frac{W(K^+_{\mu 3})}{W(K^+_{e3})} = 0.651 + 0.126\ (f_-/f_+) + 0.0189\ (f_-/f_+)^2$$

The experimental value is

$$R = 0.63 \pm 0.10$$

which gives two solutions for f_-/f_+. One solution is consistent with $f_- = 0$ and is

$$f_-/f_+ = -0.17^{+0.75}_{-0.99}$$

The other solution is not consistent with $f_- = 0$ and is

$$f_-/f_+ = -6.49^{+0.99}_{-0.75}$$

The two solutions are depicted graphically in Figure 13.

The predicted value of the τ'/τ branching ratio is 0.325, assuming the $\Delta T = 1/2$ rule is valid. The present experimental result is 0.350 ± 0.039 and is consistent with the $\Delta T = 1/2$ rule.

The predicted value of the $K_{\mu 2}$ branching ratio, assuming a universal coupling constant for the decays

$$\pi^{\pm} \to e^{\pm} + \nu \qquad K^{\pm} \to e^{\pm} + \nu$$
$$\to \mu^{\pm} + \nu \qquad \to \mu^{\pm} + \nu$$

is 0.677 ± 0.011 (see Section I.B.3). The experimental value is 0.630 ± 0.008. The theoretical value, however, does not include some theoretical corrections,[12] the most important of which is the electromagnetic correction.

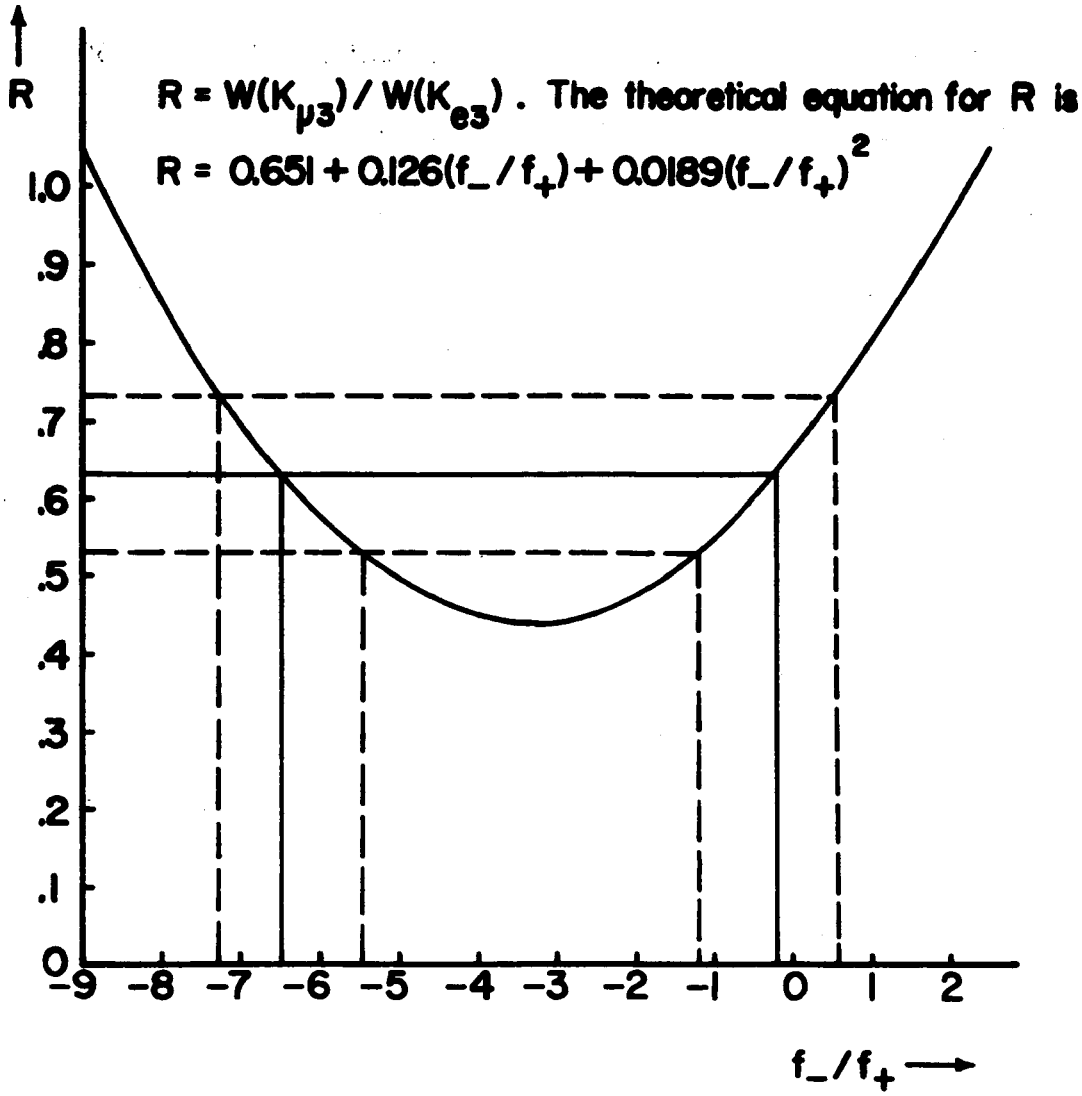


Figure 13. Experimental solution of the theoretical equation for R. Horizontal lines represent the experimental value, R = 0.63 ± 0.10.

REFERENCES

1. R. W. Birge, D. H. Perkins, J. E. Peterson, D. H. Stork and M. W. Whitehead, Nuovo cimento 4, 834 (1959).

2. G. Alexander, R.H.W. Johnson, and C. O'Ceallaigh, Nuovo cimento 6, 478 (1957).

3. S. Taylor, G. Harris, J. Orear, J. Lee, and P. Baumel. Phys. Rev. 114, 359 (1959).

4. B. P. Roe, D. Sinclair, J. L. Brown, D. A. Glaser, J. A. Kadyk, and G. H. Trilling, Phys. Rev. Letters 7, 346 (1961).

5. N. Brene, L. Egardt, and B. Qvist, Nuclear Phys. 22, 553 (1961).

6. A. Fujii and M. Kawaguchi, Phys. Rev. 113, 1156 (1959).

7. H. Chew, Phys. Rev. Letters 8, 297 (1962).

8. J. D. Jackson and R. L. Schult, University of Illinois Technical Report No. 43, Oct., 1962 (unpublished).

9. Z. Koba, Phys. Letters 1, 34 (1962).

10. R. H. Dalitz, Proc. Phys. Soc. A, 69, 527 (1956).

11. M. A. Ruderman and R. J. Finkelstein, Phys. Rev. 76, 1458 (1949).

12. M. Sugawara, Private Communication.

13. W. H. Barkas and A. H. Rosenfeld, Proc. Intern. Conf. High Energy Phys., Rochester, 1960, P. 877.

14. T. F. Stubbs, H. Bradner, W. Chinowsky, G. Goldhaber, S. Goldhaber, W. Slater, D. M. Stork, and H. K. Ticho, Phys. Rev. Letters 7, 188 (1961).

15. G. Goldhaber, S. Goldhaber, J. Kadyk, T. Stubbs, D. H. Stork, and H. K. Ticho, Lawrence Radiation Laboratory Internal Report UCID-1250, Feb. 1960 (unpublished).

16. John L. Brown, Xenon Bubble Chamber, in Proceedings of an International Conference on Instrumentation for High Energy Physics, 1960 (Interscience Publishers, Inc., New York, 1961), p. 110.

REFERENCES (Concluded)

17. J. L. Brown, H. C. Bryant, R. A. Burnstein, D. A. Glaser, R. Hartung, J. A. Kadyk, J. D. van Putten, D. Sinclair, G. H. Trilling, and J. C. Vander Velde, Nuovo cimento 19, 1155 (1961).

18. G. L. Jensen, Study of the Three-Body Leptonic Decay Modes of the K^+-Meson (Ph.D. thesis), The University of Michigan, Feb. 1964 (unpublished).

19. B. Rossi, High Energy Particles, Prentice-Hall, New York, 68 (1952).

20. G. E. Kalmus, A. Kernan, W. M. Powell, R. Dowd, and W. F. Fry, Bull. Am. Phys. Soc. Ser. II, 9, 34 (1964).

21. S. McKenna, S. Natali, M. O'Connell, J. Tietge, and N. C. Varshnaya, Nuovo cimento 10, 763 (1958).

22. R. M Sternheimer, Phys. Rev. 115, 137 (1959).

23. M. C. Walske, Phys. Rev. 101, 940 (1956).